(12) INTERNATIONAL APPLICATION PUBLISHED UNDER THE PATENT COOPERATION TREATY (PCT)

(19) World Intellectual Property Organization
International Bureau

(43) International Publication Date
23 September 2010 (23.09.2010)

PCT

(10) International Publication Number
WO 2010/108058 A2

(51) International Patent Classification:
C07D 495/04 (2006.01) *C07D 273/01* (2006.01)

(21) International Application Number:
PCT/US2010/027900

(22) International Filing Date:
19 March 2010 (19.03.2010)

(25) Filing Language: English

(26) Publication Language: English

(30) Priority Data:
61/210,643 20 March 2009 (20.03.2009) US

(71) Applicant *(for all designated States except US)*: **UNIVERSITY OF PITTSBURGH-OF THE COMMONWEALTH SYSTEM OF HIGHER EDUCATION** [US/US]; 200 Gardner Steel Conference Center, Thackeray & O'Hara Streets, Pittsburgh, Pennsylvania 15260 (US).

(72) Inventors; and

(75) Inventors/Applicants *(for US only)*: **DAY, Billy, W.** [US/US]; 1510 Scenery Ridge Drive, Pittsburgh, Pennsylvania 15241 (US). **TSANG, Waikok, Michael** [GB/US]; 1463 Barnesdal Street, Pittsburgh, Pennsylvania 15217 (US). **KOROTCHENKO, Vasiliy, N.** [RU/US]; 440 Elmcroft Blvd., Apartment 3407, Rockville, Maryland 20850 (US).

(74) Agent: **HIRSHMAN, Jesse, A.**; Gatehouse Building, Suite 500, 101 West Station Square Dr., Pittsburgh, Pennsylvania 15219 (US).

(81) Designated States *(unless otherwise indicated, for every kind of national protection available)*: AE, AG, AL, AM, AO, AT, AU, AZ, BA, BB, BG, BH, BR, BW, BY, BZ, CA, CH, CL, CN, CO, CR, CU, CZ, DE, DK, DM, DO, DZ, EC, EE, EG, ES, FI, GB, GD, GE, GH, GM, GT, HN, HR, HU, ID, IL, IN, IS, JP, KE, KG, KM, KN, KP, KR, KZ, LA, LC, LK, LR, LS, LT, LU, LY, MA, MD, ME, MG, MK, MN, MW, MX, MY, MZ, NA, NG, NI, NO, NZ, OM, PE, PG, PH, PL, PT, RO, RS, RU, SC, SD, SE, SG, SK, SL, SM, ST, SV, SY, TH, TJ, TM, TN, TR, TT, TZ, UA, UG, US, UZ, VC, VN, ZA, ZM, ZW.

(84) Designated States *(unless otherwise indicated, for every kind of regional protection available)*: ARIPO (BW, GH, GM, KE, LS, MW, MZ, NA, SD, SL, SZ, TZ, UG, ZM, ZW), Eurasian (AM, AZ, BY, KG, KZ, MD, RU, TJ, TM), European (AT, BE, BG, CH, CY, CZ, DE, DK, EE, ES, FI, FR, GB, GR, HR, HU, IE, IS, IT, LT, LU, LV, MC, MK, MT, NL, NO, PL, PT, RO, SE, SI, SK, SM, TR), OAPI (BF, BJ, CF, CG, CI, CM, GA, GN, GQ, GW, ML, MR, NE, SN, TD, TG).

Published:

— *without international search report and to be republished upon receipt of that report (Rule 48.2(g))*

— *with sequence listing part of description (Rule 5.2(a))*

(54) Title: SMALL MOLECULE INHIBITORS OF DUSP6 AND USES THEREFOR

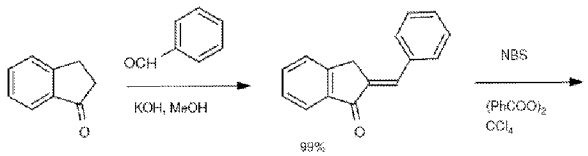

Fig. 1

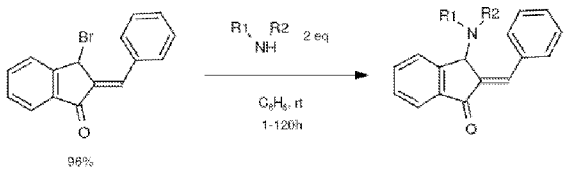

(57) Abstract: Compounds that stimulate fibroblast growth factor production, and thus cell growth are provided. Also provided are compositions comprising the compounds and methods of using the compounds. The compounds can be used to treat wounds, to expand cell populations, such as hematopoietic cells, or to grow tissue *in vitro*, among other uses.

WO 2010/108058 A2

SMALL MOLECULE INHIBITORS OF Dusp6 AND USES THEREFOR

This application claims the benefit under 35 U.S.C. §119(e) to United States Provisional Patent Application No. 61/210,643, filed March 20, 2009, which is incorporated herein by reference in its entirety.

This invention was made with government support under Grant Nos. HD053287, HL088016, CA052995, MH074411, CA078039 awarded by the National Institutes of health. The government has certain rights in the invention.

Fibroblast Growth Factors (FGFs) are members of a large family of secreted glycoproteins that serve important functions in development, proliferation and cellular homeostasis. These ligands bind to single-pass transmembrane proteins of the receptor tyrosine kinase class to activate multiple signaling pathways including the rat sarcoma homologue (RAS)/mitogen-activated protein kinase (MAPK) cascade. The wide-ranging biological roles of FGFs and the multitude of signaling pathways activated by this family of ligands suggest that FGF signaling must be tightly regulated. Dual specificity phosphatase 6 (Dusp6) (also named MAP Kinase Phosphatase 3), Sproutys (Spry1-4) and Sef (similar expression to FGFs) proteins function as RAS/MAPK pathway feedback attenuators. Through their concerted activities FGF signaling is adjusted to optimal levels in embryogenesis (Thisse, B. *et al. Dev Biol* 287, 390-402 (2005) and Tsang, M. *et al. Sci STKE* 2004, pe17 (2004)). Sef and Spry proteins suppress RAS/MAPK signaling at multiple points within the pathway, while Dusp6 inhibits the pathway only by dephosphorylation of one class of the MAPK family, extracellular signal-regulated kinase (ERK). Sef, Dusp6 and Sprouty depletion in zebrafish or gene knock-out in mice have revealed the requirement for these proteins to limit FGF signaling during development and homeostasis (Thisse, B. *et al. Dev Biol* 287, 390-402 (2005); Abraira, V.E. *et al. J Neurosci* 27, 4273-82 (2007); Li, C., *et al. Development* 134, 167-76 (2007); and Maillet, M. *et al. J Biol Chem* 283, 31246-55 (2008)). The identification of small molecules that can reversibly modulate FGF signaling would provide useful tools to dissect the roles for this pathway in development that are not feasible with current genetic methods.

SUMMARY

The dual specificity phosphatase 6 (Dusp6) functions as a feedback regulator of fibroblast growth factor (FGF) signaling to limit the activity of extracellular signal regulated kinase (ERK) 1 and 2. A small molecule inhibitor of Dusp6, (*E*)-2-benzylidene-3-(cyclohexylamino)-2,3-dihydro-1*H*-inden-1-one (BCI), was identified using a transgenic zebrafish chemical screen. BCI treatment blocked Dusp6 activity and enhanced FGF target gene expression in zebrafish embryos. Docking simulations revealed an allosteric binding site for BCI within the phosphatase domain. Studies *in vitro* supported the model that BCI inhibits Dusp6 catalytic activation by ERK2. A temporal role for Dusp6 in restricting cardiac progenitors and controlling heart organ size was uncovered with BCI treatment at varying developmental stages. Using this *in vivo* zebrafish chemical screen, several novel compounds were found to target Dusp6, a component of the FGF signaling pathway that has eluded traditional high throughput *in vitro* screens.

BRIEF DESCRIPTION OF THE DRAWINGS

Figure 1 shows a scheme for preparation of BCI and its analogs containing different amines.

Figures 2A-2C depict schemes for synthesis of compounds 14-16.

Figure 3 depicts a scheme for synthesis of compound 17.

Figure 4 depicts a scheme for synthesis of compound 18.

Figure 5 depicts a scheme for synthesis of compound 19.

Figure 6. Identification of a small molecule that activates FGF signaling in zebrafish. (**a-c**) *Tg(Dusp6:d2EFP)pt6* embryos treated with BCI (**b & b**) exhibited increased d2EGFP fluorescence as compared to DMSO (**a**). (**d-f**) Embryos treated with BCI during gastrulation had expanded *ntl* expression at the 6-somite stage (**e & f**). (**g & h**) *dusp6 mRNA* was increased in BCI treated embryos. Note that the MHB, r4 and somites showed stronger *dusp6* staining (**h**) than in DMSO treated (**g**). Red arrowheads demarcate the MHB. (**i & j**) BCI treatment during somitogenesis stages expanded the MHB and r3 and r5, as marked by *eng3* and *krox20* expression, respectively (**j**). (**k**) BCI treatment induced expression of the FGF target genes *sef* and *spry4* as measured by RT-PCR. Histone H4 served as RNA loading control. (**l**) The chemical structure of BCI.

Figure 7. BCI structure-activity relationship studies. (**a-d**) Lateral views of 30hpf embryos treated with the compounds shown. d2EGFP fluorescence was enhanced in BCI-treated embryos (**b**), while related analogs, shown in inner panels, had no effect, even at four-fold higher concentrations (**c & d**). Red arrowheads label the MHB.

Figure 8. BCI does not hyperactivate FGF signaling in the absence of ligand and suppresses dusp6 over-expression. (**8a-8d**) Lateral views of 24hpf embryos. *Tg(Dusp6:d2EGFP)pt6* embryos (**8a and 8b**) or *Tg(Dusp6:d2EGFP)pt6;ace* (**8c and 8d**) were treated with BCI (10μM). The *ace* mutants do not show induction of d2EGFP within the MHB (red arrows) where FGF ligands are not present (**3d**). (**3e-3m**) Lateral views of shield stage embryos showing *sef* expression by *in situ* hybridization. Red brackets demarcate *sef* expression domain. Injection of *dusp6*, *spry4* or *dusp5* reduced *sef* expression (**3f, 3i and 3l**). BCI treatment restored *sef* expression in *dusp6*-injected embryos (**i**), but not in embryos injected with spry4 or dusp5 (**8j and 8m**). (**8n**) Graph depicting injection and BCI treatment results. *Sef* expression in mRNA-injected embryos is represented by color bars that denote normal (WT) expression in blue, weaker (-) expression in yellow and absent (--) expression in green.

Figure 9. Ectopic expression of XFD blocks FGF signaling that is not reversed by BCI (**a-c**) Lateral view of Shield stage embryos stained showing *sef* expression as a marker for FGF activity. (a) uninjected control. (b) Embryo injected with *XFD* mRNA shows a marked reduction of *sef* expression. (c) Embryo injected with *XFD*, followed by incubation with 5μM BCI did not restore *sef* expression.

Figure 10. BCI directly inhibits Dusp6 in both chemical complementation and in pERK2 dephosphorylation assays. (**a-d**) Cell-based chemical complementation assay. TPA stimulation of HeLa cells induced ERK phosphorylation (red cells in **a & b**). In cells overexpressing Dusp6-Myc (green cells in

c), p-ERK was abolished (green cells in **c & d** are outlined yellow cells in **a & b**). In the presence of BCI, pERK levels remained high (red cells in **b**), even in cells expressing high levels of Dusp6-Myc (outlined yellow cells in **b**). (**e**) Quantification of pERK levels in Dusp expressing cells. Cells expressing high levels of Dusp6 (upper panel) or Dusp1 (lower panel) were identified based on c-Myc immunostaining and analyzed for ERK phosphorylation using Kolmogorov-Smirnov (KS) statistics as described in Materials and Methods. pERK levels were normalized to Dusp transfected and vehicle treated cells. BCI inhibited Dusp6 and Dusp1 with IC50 values of 16.0 μM and 11.2 μM, respectively. Data are the averages ± SD of quadruplicates from a single experiment that was repeated six times with similar results. (**f**) p-ERK2 *in vitro* dephosphorylation assay shows BCI (100μM) specifically suppressed Dusp6 activity (lane 4) while a related analog, ICD (100μM) did not (lane 5).

Figure 11. BCI does not inhibit Cdc25B (11A), PTP1B (11B) or Dusp3/VHR (11C). Recombinant enzymes were incubated with OMFP in the presence of increasing concentration of BCI (15.2nM - 300μM). BCI exhibited no activity in suppressing phophatase activity by these enzymes. Assays were performed in triplicates (individual graph represents a single experiment) for each phosphatase. Sodium orthovanadate (100μM) completely inhibited all three phosphatases and represented 100% inhibition.

Figure 12. BCI does not inhibit dephosphorylation of OMFP by Dusp6 (a) BCI did not suppress Dusp6 basal phosphatase activity toward OMFP. NSC95397 (2,3-bis(2-hydroxyethylthio)naphthalene-1,4-dione), a broad spectrum dual specificity phosphatase inhibitor, blocked basal Dusp6 activity toward OMFP. (**b**) A 10-fold excess of ERK2 (2.1μg) stimulated (210ng) Dusp6 dephosphorylation of OMFP by 6.5-fold and this induction was blocked by BCI. RFU, Relative Fluorescent Units were measured at excitation/emission wavelengths of 485/525nm.

Figure 13. Testing *in vitro* of the allosteric inhibition mechanism. ERK2 stimulated Dusp6 dephosphorylation of OMFP; and this induction was blocked by BCI. RFU, Relative Fluorescent Units were measured at excitation/emission wavelengths of 485/525nm.

14. Dusp6 and FGFs regulate heart size. (**a-h & k-m**) Hybridization *in situ* of treated embryos as indicated. (**a, b, a', b'**) BCI treatment expanded *gata4* expression in the caudal ALPM; blue box and brackets mark ALPM and caudal cardiac domain, respectively. (**c & d**) BCI increased *nkx2.5* expression and expanded cardiac progenitor populations. (**e & f**) Fluorescent double *in situ* hybridization showing *scl* (green) and *hand2* (red) expression in BCI-treated embryos. Reduction of *scl* expression with a concomitant expansion of *hand2* in BCI-treated embryos (**F**). Red and green bracket show expression domains. (**g & h**) *cmlc2* expression in 18-somite stage embryos showed an increase in cardiomyocytes in BCItreated embryos. (**i & j**) Larvae at 56hpf treated with BCI (from 40% epiboly for 8 hours) exhibited an enlarged heart. Red outline shows heart. These phenotypes correspond to expansion of *vmhc* (compare **l** to **k** and *cmlc2* (compare **n** to **m**) staining (red arrowheads). (**o**) Graph showing temporal inhibition of Dusp6 from gastrula to somitogenesis stages resulted in cardiac expansion.

Figure 15. BCI treatment from gastrula stage onwards resulted in enlarged hearts (a & b) Graph showing BCI treatment resulted in cardiac expansion as measured by *cmlc2* and *vmhc* expression. Note that by the 8-somite stage, the ability of BCI to induce heart expansion was reduced.

Figure 16 shows BCI expanded GFP expression in transgenic embryos. The EC_{50} was measured as 11.4μM.

Figure 17 shows toxicity and EC_{50} for selected BCI analogs in zebrafish.

DETAILED DESCRIPTION

The use of numerical values in the various ranges specified in this application, unless expressly indicated otherwise, are stated as approximations as though the minimum and maximum values within the stated ranges are both preceded by the word "about". In this manner, slight variations above and below the stated ranges can be used to achieve substantially the same results as values within the ranges. Also, unless indicated otherwise, the disclosure of these ranges is intended as a continuous range including every value between the minimum and maximum values. For definitions provided herein, those definitions also refer to word forms, cognates and grammatical variants of those words or phrases.

As used herein, the terms “comprising,” “comprise” or “comprised,” and variations thereof, in reference to elements of an item, composition, apparatus, method, process, system, claim *etc.* are intended to be open-ended, meaning that the item, composition, apparatus, method, process, system, claim *etc.* includes those elements and other elements can be included and still fall within the scope/definition of the described item, composition, apparatus, method, process, system, claim *etc.* As used herein, "a" or "an" means one or more. As used herein "another" may mean at least a second or more.

As used herein, the terms "patient" or "subject" refer to members of the animal kingdom including but not limited to human beings.

The dual specificity phosphatase Dusp6 is a mitogen-activated protein kinase (MAPK) phosphatase, also known as MKP3, that functions as a feedback regulator of fibroblast growth factor (FGF) signaling to limit the activities of the extracellular regulated kinase ERK2. A small molecule inhibitor of Dusp6, (*E*)-2-benzylidene-3-(cyclohexylamino)-2,3-dihydro-1*H*-inden-1-one (BCI), was identified from a zebrafish chemical screen. Treatment with BCI blocked Dusp6 activity and expanded FGF target gene expression in the embryo as visualized with green fluorescent protein-labeled gene products. Herein, we report the design, synthesis, biological activity and structure-activity relationships (SAR) of BCI analogs. Syntheses of affinity versions of BCI will be disclosed.

The zebrafish embryo is a vertebrate animal model well-suited for high-content small molecule screening (Zon, L.I. *et al. Nat Rev Drug Discov* 4, 35-44 (2005) and Vogt, A. *et al. Dev Dyn* 238, 656-663 (2009)). Due to its small size, rapid development and ease of handling it is possible to identify compounds that affect developmental processes and chemical modulators of signaling pathways *in vivo* (Zon, L.I. *et al. Nat Rev Drug Discov* 4, 35-44 (2005) and Peterson, R.T., *et al. Proc Natl Acad Sci U S A* 97, 12965-9

(2000)). Previous zebrafish chemical screens have relied on the observations of phenotypes generated by small molecules treatment. In one phenotypic screen, Dorsomorphin was identified as an inhibitor of Bone Morphogenetic Protein (BMP) as embryos exhibited patterning defects upon chemical treatment and subsequent studies utilizing Dorsomorphin in mice have revealed the importance of the BMP pathway in regulating iron metabolism (Yu, P.B. *et al. Nat Chem Biol* 4, 33-41 (2008)). Another example of the relevance of zebrafish screens was the discovery that Prostaglandin E2 is a key regulator of haematopoietic stem cells (HSC) homeostasis. These studies have shown that this pathway is conserved in vertebrates and provide the potential for using molecules to expand HSC to restore blood deficiencies in patients (North, T.E. *et al. Nature* 447, 1007-11 (2007)).

The generation of transgenic reporter lines in zebrafish offers alternative *in vivo* tools for chemical screening. Reporters for FGF signaling have been generated and allow for the live visualization of signaling activity during early development. Here, a chemical screen was performed with an FGF reporter transgenic line and identified a small molecule, (*E*)-2-benzylidene-3-(cyclohexylamino)-2,3-dihydro-1*H*-inden-1-one (BCI), that hyperactivated FGF signaling. Further analyses revealed that BCI blocked Dusp6 activity in zebrafish embryos and in cultured cells. Molecular modeling predicted an energetically favorable site for BCI binding on Dusp6 phosphatase domain and suggested a plausible allosteric mechanism of action, which was supported by *in vitro* assays. In one non-limiting example, described below, using BCI as a chemical probe, it was revealed that inhibition of Dusp6 activity during somitogenesis expanded cardiac progenitors at the expense of endothelial lineages. This example suggests that Dusp6 functions, at least in one instance, as an attenuator of FGF signaling in the cardiac field to regulate heart organ size. Further studies, also described below, indicate that a number of analogs of BCI have equal or better activity.

Thus, provided herein are compounds having the general formula:

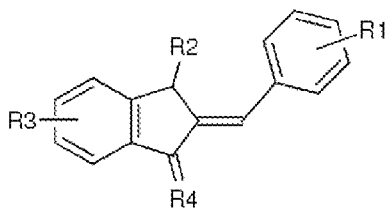

where R1 and R3 represent one or more independently of H, halo, C_{1-3} alkyl, C_{1-3} alkoxyl or –CN; R2 is a primary or secondary amine (-NRH or –NRR', forming, when incorporated into the compound, a secondary or tertiary amine); and R4 is =O or –OH. In one embodiment, when R1 and R3 are H (that is, the aryl rings containing R1 and R3 contain only hydrogens) and R4 is =O, R2 is not cyclohexylamine, cyclophenylamine, piperidine or morpholine. In one example, the compound has the formula:

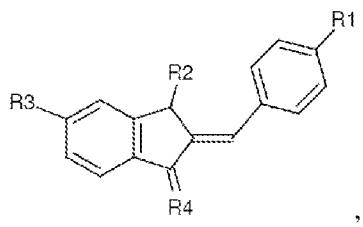

,

with R1, R2, R3 and R4 defined as indicated above.

Examples of such compounds are depicted in Table 1, below. In one example, R3 is halo, that is, the ring to which R3 is attached may comprise one or more, independently, halo groups, e.g., F, Cl, Br and I. In one example, R3 is Br (a single Br). In another example, R2 is a C_{4-10} cycloalkylamine, including cyclobutylamine, cyclopentylamine, cyclohexylamine, cycloheptylamine, cyclooctylamine, cyclononylamine, and cyclodecylamine, for example, R2 may be cyclopentylamine or cycloheptylamine, or R1 is H, R2 is one of cyclopentylamine, cyclohexylamine, and cycloheptylamine, and R3 is Br. In one non-limiting embodiment, R1 is halo or dihalo, for example, 4-chloro or 3,4-dichloro.

Table 1. BCI analogs

1	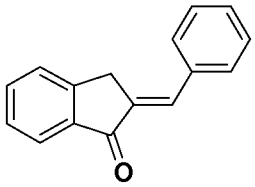	20 VNK-I-211B CSA	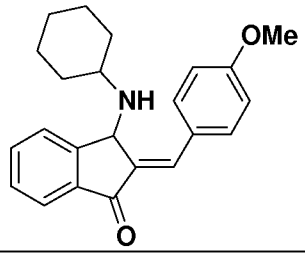
2	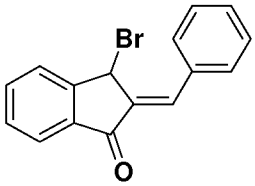	20a VNK-I-211A CSA	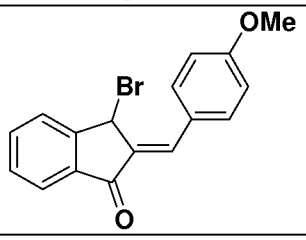
3 (BCI)	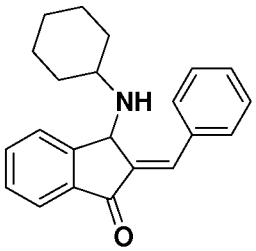	21 VNK-I-212 KG-17-C2	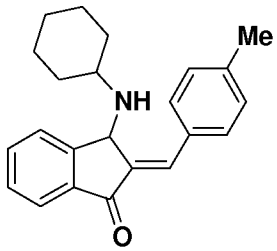
(+)-BCI	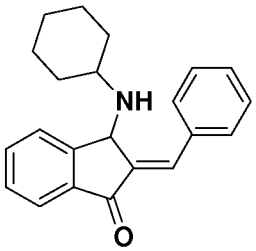	21a	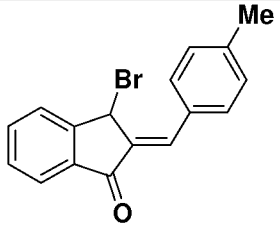
(-)-BCI	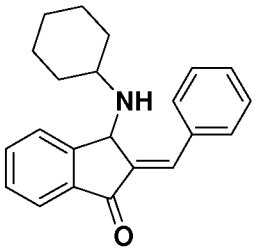	22 VNK-I-215 KTD	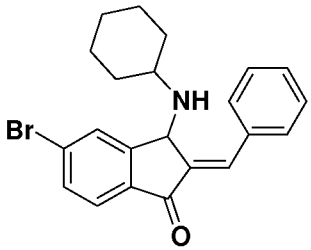

4 VNK-I-164	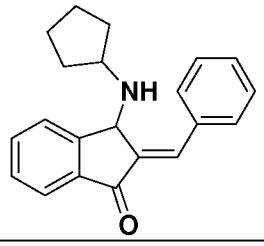	22a	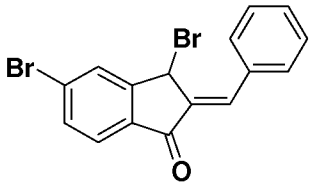
5 VNK-I-165	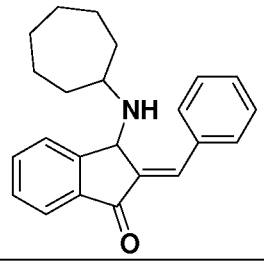	23 VNK-I-216 KTD	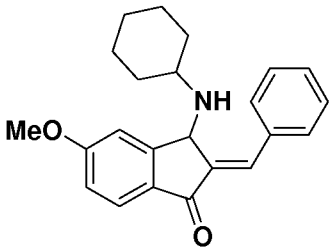
6 VNK-I-149	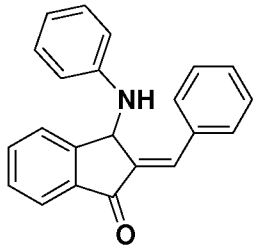	23a VNK-I-216a KTD	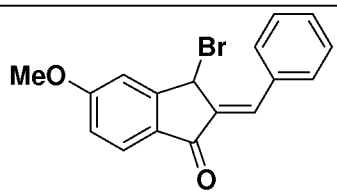
7 VNK-I-147	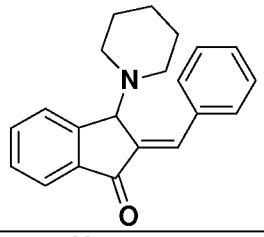	24 VNK-I-217 CSA	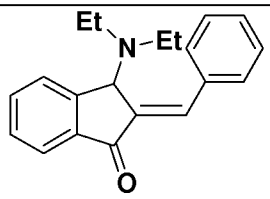
8 VNK-I-53	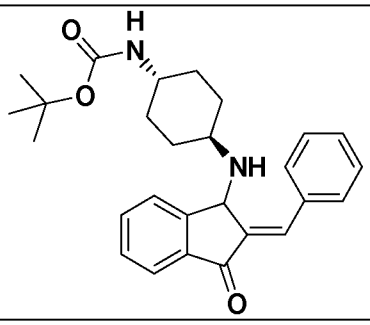	25a	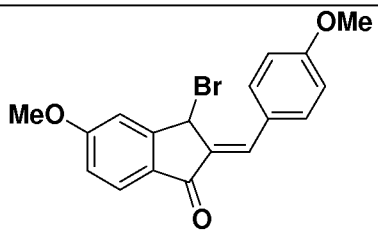
9 VNK-I-148	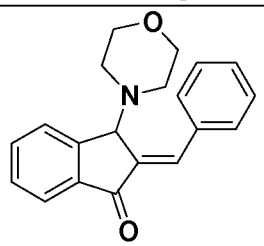	25b	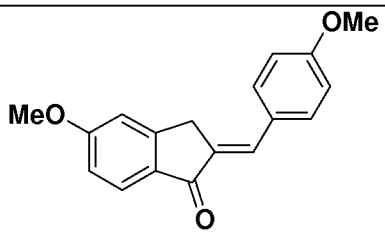
10 VNK-I-177	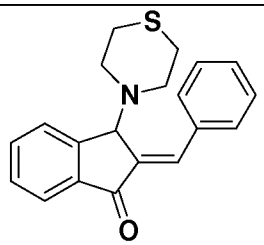	25	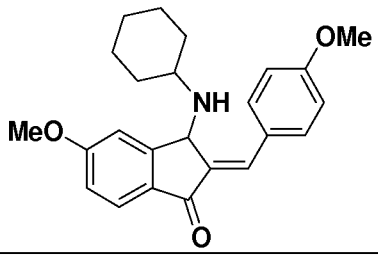

11 VNK-I-187	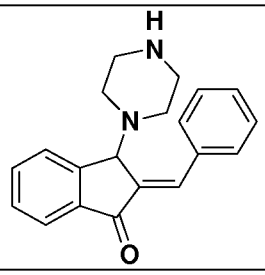	26	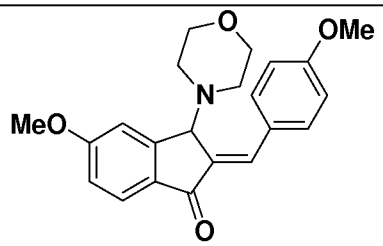
12 VNK-I-178	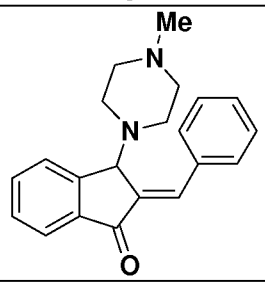	27	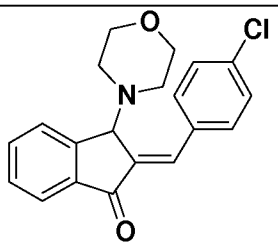
13 VNK-I-179	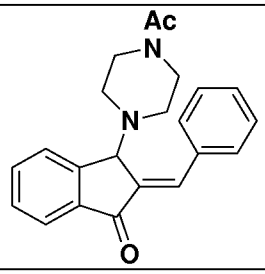	28a	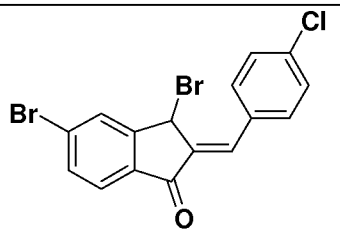
14 VNK-I-183	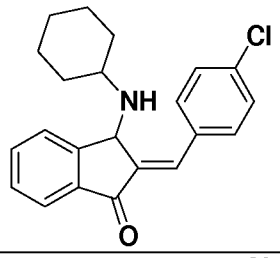	28b	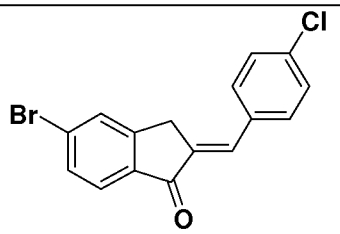
14a	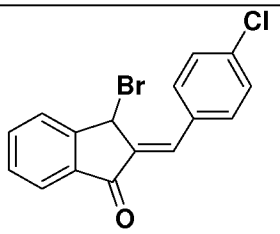	28	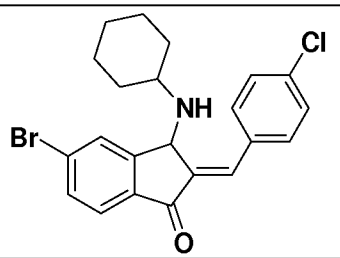
15 VNK-I-137	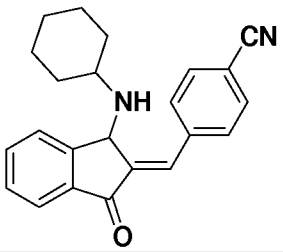	29	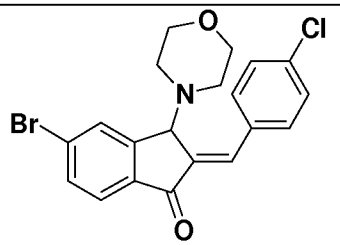
15a VNK-I-132	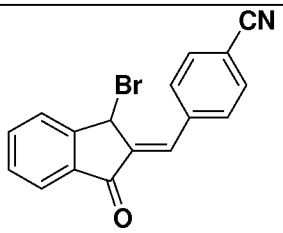	30	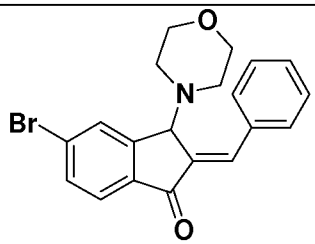

16 VNK-I-169	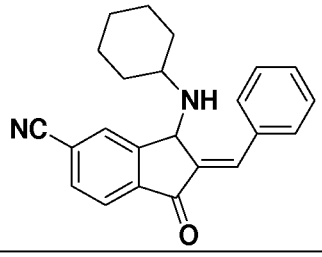	31a	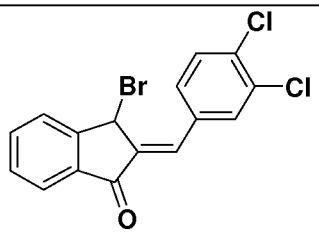
16a	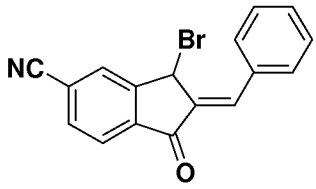	31	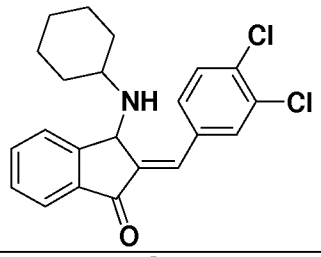
17 WD compound	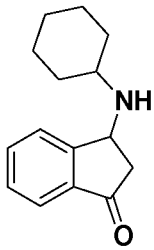	32	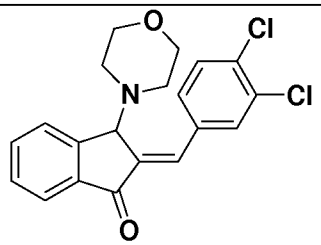
18 VNK-I-146	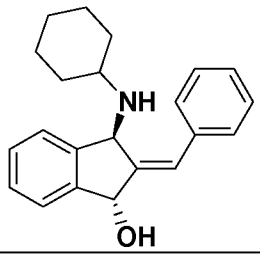		
19 VNK-I-107	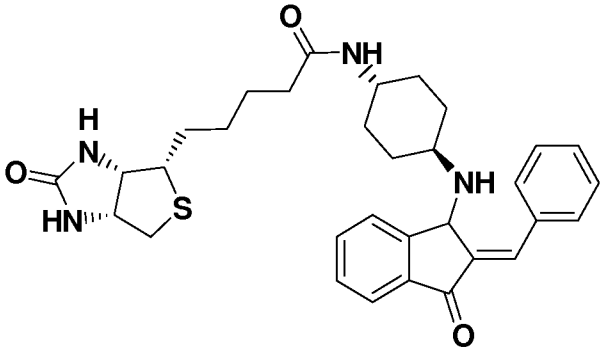		
19b	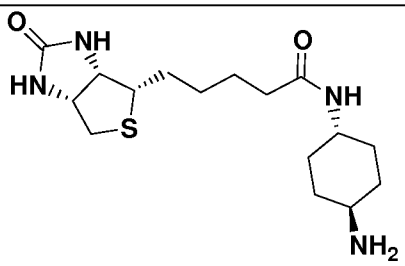		

The compound may be an enantiopure preparation consisting essentially of an (-) or (+) enantiomer of the compound, for example (-) BCI or (+)BCI, or may be a mixture of enantiomers in either equal (racemic) or unequal proportions.

In one non-limiting embodiment of the compounds, R4 is =O. Additional examples of R2 include: *t*-Boc-cyclohexylamine, thiamorpholine, piperazine, methyl piperazine, acetyl piperazine, cyclopentylamine, cycloheptylamine and di-C_{1-4}-alkylamine.

A compound consisting of a (-) enantiomer of a compound having the formula:

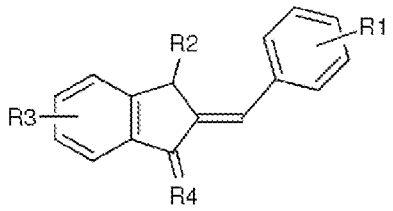

in which R1 represents one or more independently of H, halo, C_{1-3} alkyl, C_{1-3} alkoxyl or –CN; R2 is a primary or secondary amine; R3 is one or more independently of H, halo, C_{1-3} alkyl, C_{1-3} alkoxyl or –CN; and R4 is =O or –OH.

As used herein, a ring structure showing a bond/group that is not attached to any single carbon atom, for example and without limitation, depicted as 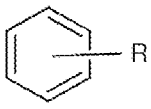

, can be substituted at any position with one or more groups designated "R", and, unless indicated otherwise, each instance of R on the ring can be (independently) the same or different from other R moieties on the ring. Thus, if R is H, the group contains nothing but H groups. If R is "halo", it is a single halo (e.g., F, Cl, Br and I) group. If R is one or more independently of halo and CN, the ring may comprise one, two, three, four, halo or CN groups, such as, for example and without limitation: 2, 3, 4, or 5 chloro; 2, 3, 4, or 5 bromo; 2, 3- or 3,4- or 4,5- or 2,4-dichloro; 3-bromo-4-chloro; 3-bromo-4-cyano, and any other possible permutation of the listed groups. Unless otherwise indicated, the described compounds include all stereoisomers or enantiomers and include preparations comprising one enantiomer (enantiopure compositions) and mixtures of enantiomers, such as racemic mixtures.

Also provided is a composition comprising one or more compounds of any one of claims 1-15 and a solvent or carrier, such as a pharmaceutically acceptable excipient. The compounds may be compounded or otherwise manufactured into a suitable composition for use, such as a pharmaceutical dosage form or drug product in which the compound or compounds are an active ingredient. Compositions may comprise a pharmaceutically acceptable carrier, or excipient. An excipient is an inactive substance used as a carrier for the active ingredients of a medication. Although "inactive," excipients may facilitate and aid in increasing the delivery or bioavailability of an active ingredient in a drug product. Non-limiting examples of useful excipients include: antiadherents, binders, rheology modifiers, coatings, disintegrants, emulsifiers, oils,

buffers, salts, acids, bases, fillers, diluents, solvents, flavors, colorants, glidants, lubricants, preservatives, antioxidants, sorbents, vitamins, sweeteners, etc., as are available in the pharmaceutical/compounding arts.

Useful dosage forms include: intravenous, intramuscular, or intraperitoneal solutions, oral tablets or liquids, topical ointments or creams and transdermal devices (e.g., patches). In one embodiment, the compound is a sterile solution comprising the active ingredient (drug, or compound), and a solvent, such as water, saline, lactated Ringer's solution, or phosphate-buffered saline (PBS). Additional excipients, such as polyethylene glycol, emulsifiers, salts and buffers may be included in the solution. In one embodiment, the composition is an injectable solution or gel, which is injected at a site in which cell growth is desired, such as at the site of a wound or defect. The composition may be a topical composition, such as a lotion, cream or ointment for use in wound healing, where the topical composition is applied to a wound, such as a cut or burn.

The compounds include pharmaceutically acceptable salts. Pharmaceutically acceptable salts are, because their solubility in water is greater than that of the initial or basic compounds, particularly suitable for medical applications. These salts have a pharmaceutically acceptable anion or cation. Suitable pharmaceutically acceptable acid addition salts of the compounds of the invention include, without limitation, salts of inorganic acids such as hydrochloric acid, hydrobromic, phosphoric, metaphosphoric, nitric and sulfuric acid, and of organic acids such as, for example, acetic acid, benzenesulfonic, benzoic, citric, ethanesulfonic, fumaric, gluconic, glycolic, isethionic, lactic, lactobionic, maleic, malic, methanesulfonic, succinic, *p*-toluenesulfonic and tartaric acid. Suitable pharmaceutically acceptable basic salts include without limitation, ammonium salts, alkali metal salts (such as sodium and potassium salts), alkaline earth metal salts (such as magnesium and calcium salts), and salts of trometamol (2-amino-2-hydroxymethyl-1,3-propanediol), diethanolamine, lysine or ethylenediamine. Pharmaceutically acceptable salts may be prepared from the described compounds by any useful method, as are well known in the chemistry and pharmaceutical arts.

Also provided is a method of stimulating (e.g., inducing, increasing, up-regulating, etc.) cell growth in a population of cells -that is, in a culture of one or more cells, in a tissue, in an *in vitro* or *ex vivo* cell preparation obtained from a patient and optionally for replacement in the patient opr in another patient, in an organ, in an organism, etc. The method comprises contacting the cell population with a compound described herein in an amount effective to increase FGF secretion by the cell. In one embodiment, the method comprises applying the compound to a tissue in an organism, e.g., of a patient. In one embodiment, the tissue of the organism is damaged or deficient (e.g.,is a wound or congenital defect). In another embodiment, the method can be used to expand a cell population or grow a tissue of a patient. For example, the method comprises obtaining cells from a patient and contacting the cells *in vitro* with the compound to expand the population of cells.

The compounds described herein can be readily synthesized by those of ordinary skill. The BCI molecule has four distinct sites of modification (R1, R2 and R3, and the carbonyl group, R4). BCI and its analogs containing different amines were synthesized following the general procedure depicted in Figure 1. Briefly, condensation of 1-indanone with benzaldehyde is followed by bromination of benzylideneindanone (compound 1) provides 3-bromo-2-benzyliden-1-indanone (compound 2), a general precursor for the family of analogs. Treatment of compound 2 with 2 eq of primary or secondary amines provided analogs 3-13 in high yield.

Variations using substituted indanones or benzaldehydes provided easy access to other BCI analogs, such as compounds 14, 15 and 16 (See, Figures 2A-2C). Bromination of 1-indanone and treatment of bromoindanone with cyclohexylamine provided analog 17 (ICD), which lacks the benzylidene group (see Figure 3). LAH reduction of BCI resulted in formation of amino alcohol 18 with a *trans* relationship between the amine and hydroxy groups (see Figure 4). Compound 19, which contained biotin linked to ring A, was prepared from compound **2** and the easily available monobiotinylated diaminocyclohexane (see Figure 5). Additional synthesis schemes are described in the Examples.

Example 1 - (*E*)-2-benzylidene-3-(cyclohexylamino)-2,3-dihydro-1*H*-inden-1-one (BCI) enhances FGF signaling

Zebrafish chemical screens.

Tg(dusp6:d2EGFP)pt6 embryos were obtained by natural crossings and incubated at 28.5oC until they reached 24hpf. Five transgenic embryos were placed into each well from a 96-well plate in 200µl of E3, and a 0.5% DMSO solution was added along with compound from each library at 10µM. The NCI diversity set (NCI/NIH), the Natural Products library (MicroSource Discovery Systems Inc.) and Phosphatase targeted set (Chembridge) were screened in this study. (*E*)-2-Benzylidene-3-(cyclohexylamino)-2,3-dihydro-1*H*-inden-1-one (BCI; also known as NSC150117) was identified as a compound that enhanced fluorescence in treated transgenic embryos. Treated embryos were photographed under the same settings for exposure, gain and magnification for each picture using a MZFLIII (Leica) microscrope and fluorescent illumination for GFP using endow cube (Chroma Technology Corp., Rockingham, VT). Qimaging software and the Retiga Exi camera (Qimaging, Burnaby, BC Canada) were used to capture the images. Each experiment was repeated three times to show reproducibility of the assay and at least four of the five treated embryos exhibited the same phenotype.

Zebrafish RNA microinjection

dusp6 and *XFD mRNA* for microinjection studies were generated as previously described (Tsang, M. *et al. Development* 131, 2769-79 (2004)). Both Dusp5 and Spry4 ORFs were amplified by RT-PCR from 24hpf zebrafish with the following primers:

Dusp5 Forward: 5'-AACTCGAGGCCATGAAGGTCTCCAGCATAGATTGCCG-3' (SEQ ID NO: 1)

Dusp5 Reverse: 5'-AATCTAGATTAAGGCAGCGCAGTTATTGGACTC-3' (SEQ ID NO: 2)

Spry4 Forward: 5'-ACTCGAGCCATGGAGTCAAGGGTTCCTCACCACATTC-3' (SEQ ID NO: 3)

Spry4 Reverse: 5'-AATCTAGATCATGAGGCTTGTTTTTCTGGCTGAC-3' (SEQ ID NO: 4)

Amplified PCR products were subcloned into pCS2+, sequenced verified and mRNAs were synthesized as described previously. Embryos were injected with 500pg mRNA at the 1-2 cell stage, treated with 5μM BCI at the 1000-cell stage and fixed at shield stage for *in situ* hybridization.

Chemical complementation assays in HeLa cells.

These experiments were carried out essentially as described26. HeLa cells were obtained from ATCC (Manassas, VA) and maintained in a humidified atmosphere of 5% CO2 at 37oC, Dulbecco's Minimum Essential Medium (DMEM) supplemented with 10% fetal bovine serum (FBS, HyClone, Logan, UT), and 1% penicillin-streptomycin (Life Technologies, Inc., Rockville, MD). c-Myc-Dusp6 and c-Myc-Dusp1 (also known as CL100) (kindly provided by Dr. Stephen Keyse, University of Dundee) were subcloned into pcDNA3.1 for ectopic expression in mammalian cells50. HeLa cells (2,000) were plated in the wells of a collagen-coated 384-well plate (Falcon Biocoat) in the presence of FuGene 6 (Roche Biosciences) and c-Myc-Dusp6 or c-Myc-Dusp1 as described26. After 20h in culture, cells were treated in quadruplicate wells for 15 min with ten two-fold concentration gradients of BCI or phenylarsine oxide (PAO) and stimulated for 15 min. with TPA (500 ng/ml). Cells were fixed and stained with Hoechst 33342 in 4% formaldehyde, permeabilized, and immunostained with a mixture of anti-pERK (1:200 dilution, Cell Signaling Technology) and anti-c-Myc (1:100 dilution, Santa Cruz Biotechnology) antibodies. Positive pERK and c-Myc-DUSP signals were visualized with AlexaFluor-594 (pERK) and Alexa-488 (c-Myc) conjugated secondary antibodies, respectively. Plates were analyzed by three-channel multiparametric analysis for p-ERK and c-Myc-DUSP intensities in an area defined by nuclear staining using the Compartmental Analysis Bioapplication on an ArrayScan II high-content reader (Cellomics, Pittsburgh, PA). Restoration of ERK phosphorylation by BCI in Dusp6 overexpressing cells was quantified by Kolmogorov-Smirnov (KS) statistics as described previously using DUSP-transfected and vehicle treated control wells26. One thousand individual cells were gated for Dusp-Myc expression based on c-Myc immunostaining and analyzed for ERK phosphorylation. A pERK cumulative distribution function (cdf) was established for each condition and compared to a reference cdf from Dusp-Myc expressing and vehicle-treated cells. High KS values denote large differences in ERK phosphorylation levels compared with vehicle control and indicate suppression of Dusp activity. To quantify restoration of Erk phosphorylation in the Dusp expressing cells after compound treatment, KS values for each condition were normalized to the average KS value from four wells transfected with Dusp1 or Dusp6 and treated with vehicle. Detail material and methods on *in vitro* phosphatase assays and chemical synthesis of BCI and related analogs are listed in Supplementary Methods online.

RT-PCR

Zebrafish embryos were treated at 24hpf for 6 hours with BCI at 10μM and 20μM followed by total RNA extraction with Trizol (Invitrogen). cDNA synthesis with SuperScript II Reverse Transcriptase (Invitrogen) was performed as described by manufacture's protocol and by Tsang et al.17. For PCR reaction, HotMaster Taq (Eppendorf) was used with the following primers:

Dusp6: For 5'-CGTTCAGAGGGGTTGTCCG-3' (SEQ ID NO: 5)

Dusp6: Rev 5'-CTTCCCTGAACAGGAGACCC-3' (SEQ ID NO: 6)

Spry4: For 5'-GCGGAGCAGCCCAAGATACT-3' (SEQ ID NO: 7)

Spry4: Rev 5'-CAGGCAGGGCAAAACCAATGAG-3' (SEQ ID NO: 8)

Sef: For 5'-CCAGTCAGGACGCGGGTTCAT-3' (SEQ ID NO: 9)

Sef: Rev5'-GTTAAAGTGGCGCTGCGAGTGGAG-3' (SEQ ID NO: 10)

Histone H4: For 5'-CACGAAACCCGCCATCCGTCG-3' (SEQ ID NO: 11)

Histone H4: Rev 5'-GTACAGAGTGCGTCCCTGCCG-3' (SEQ ID NO: 12)

Cycle conditions were: 94°C 30sec, 55°C 45sec, 72°C 40sec, for 25 cycles. PCR products were resolved on 3% agarose gels.

Whole mount *in situ* hybridization

In situ hybridization experiments were carried out as described previously (Kudoh, T. *et al. Genome Res* 11, 1979-87 (2001)). The probes *eng3*, *krox20*, *sef*, *dusp6*, *gata4*, *nkx2.5*, *cmlc2*, *vmhc*, *scl*, *etsrp* and *hand2* were generated with a RNA labeling kit (Roche)(Tsang, M. *et al. Development* 131, 2769-79 (2004); Chen, J.N. *et al. Development* 122, 3809-16 (1996); Ekker, M., *et al. Development* 116, 1001-10 (1992); Liao, E.C. *et al. Genes Dev* 12, 621-6 (1998); Oxtoby, E. *et al. Nucleic Acids Res* 21, 1087-95 (1993); Pham, V.N. *et al. Dev Biol* 303, 772-83 (2007); Tsang, M., *et al. Nat Cell Biol* 4, 165-9 (2002); Yelon, D., *et al. Dev Biol* 214, 23-37 (1999); and Yelon, D. *et al. Development* 127, 2573-82 (2000)). The double fluorescent *in situ* hybridization protocol was described by Schoenbeck *et al.* (*Dev Cell* 13, 254-67 (2007)). Fluorescent *in situ* hybridizations were visualized by confocal microscopy. Single optical sections and z-series of flat-mounted stained embryos were collected with a confocal laser scan head (SP5, Leica Microsystems, Inc.) mounted on an inverted compound microscope (DMI6000, Leica Microsystems, Inc.). Images were scanned and compiled with NIH ImageJ software (rsb.info.nih.gov/ij/).

Phosphatase assays *in vitro*.

ERK dephosphorylation assays were performed as described previously with several modifications (Lazo, J.S. *et al. J Pharmacol Exp Ther* 322, 940-7 (2007)). Briefly, recombinant His-tagged Dusp6 (1.5ng) was incubated for 20 minutes at 25°C in the presence of 100μM BCI, 100μM ICD or 1mM sodium orthovanadate. Tyrosine and threonine phosphorylated ERK2 (New England Biolabs; 10ng) was added and reaction mixture (30mM Tris-HCl, pH 7.0, 75mM NaCl, 0.67mM EDTA, 1mM DTT and 0.033% bovine serum albumin) was incubated at 25°C for a further 60 min. ERK desphosphorylation was determined by Western blotting using 10% Tris-glycine gels and a monoclonal phospho-p44/42 MAPK antibody (Cell Signaling) at 1:1000 dilution. Total ERK was measured as a loading control using an anti-ERK antibody (Cell Signaling).

Cdc25B, PTP1B and VHR assays *in vitro*

Enzyme activities in the presence or absence of BCI were measured using the artificial substrate 3-*O*-methylfluorescein (OMFP) at concentrations equal to the Km of each enzyme (Cdc25B, PTP1B &

Dusp3/VHR) and at optimal pH for individual enzyme activity in a 96-well microtiter plate assay based on previously described methods by Lazo et al. (*J Med Chem* 44, 4042-9 (2001) and Lazo, J.S. *et al. Bioorg Med Chem* 14, 5643-50 (2006)). Briefly, the standard assay conditions contained 0.02 mg/ml OMFP in assay buffer (30mM Tris-HCl (pH8.0), 75mM NaCl, 1mM EDTA, 0.33% BSA and 1mM DTT). Fluorescence emission was measured after a sixty-minute incubation period at ambient temperature using a multiwell plate reader (SpectraMax m5, Applied Biosystems; excitation 485nm, emission 525nm). Sodium orthovanadate (100μM) was used as a positive control for full phosphatase inhibition. IC50 concentrations were determined from three experiments using 10 concentrations of BCI ranging from 300μM to 15.2nM and GraphPad Prism 5.0 software.

For OMFP based ERK2 induced activation of Dusp6, recombinant His-tagged Dusp6 was expressed from a bacterial expression vector and 250ng were incubated with the indicated concentrations of NSC95397 or BCI. OMFP was added at its apparent Km (100 μM)(Vogt, A. *et al. J Biol Chem* 280, 19078-86 (2005)). The final reaction volume was 15μl. After 1 h at RT, OMF fluorescence was measured on an M5 multimode reader (Molecular Devices) at excitation/emission wavelengths of 485/525nm. To assay activated Dusp6, 210ng or 2.1μg of recombinant ERK2 (Cell signaling) were added to Dusp6(210ng)/BCI(100μM) mixtures to measure activation at 1:1 and 1:10 ratio of substrate to enzyme. OMFP was immediately added and fluorescence (ex485/em525nm) was read every 10 min for 130 min. Fold activation was calculated at 60mins in each experiment.

Docking Simulations

A two-step process was adopted for predicting the optimal binding poses of BCI and assessing the potential mechanism of inhibition. First, unbiased docking simulations were performed where the target protein (Dusp6) was assumed to be rigid either in the low-activity state or the high-activity state. These simulations permitted us to build two hypotheses, one of which was supported by more detailed flexible docking simulations. The method and results from the two successive steps are described in more details.

Results

A transgenic zebrafish screen identifies a small molecule activator of FGF signaling

We previously described the generation of a transgenic zebrafish line, (*Tg(Dusp6:d2EGFP)pt6*) that expresses destabilized green fluorescent protein (d2EGFP) under the control of FGF signaling (Molina, G.A., *et al. BMC Dev Biol* 7, 62 (2007)). Using *Tg(Dusp6:d2EGFP)* embryos as a biosensor for FGF signaling, we screened over 5000 diverse compounds assembled from chemical libraries for small molecule modulators of this pathway. Five transgenic embryos at 24 hours post fertilization (hpf) were arrayed into each well of a 96-well plate containing test compounds at 10 μM. d2EGFP intensity in treated embryos was visually analyzed and compared to vehicle control (0.5% DMSO) after 6-8 hours. BCI enhanced d2EGFP fluorescence in a concentration-dependent manner and was detected as early as 2 hours post treatment (Figure 6a-c). To confirm that BCI hyperactivated FGF signaling, we treated embryos prior to gastrulation (5hpf), and we analyzed by whole mount *in situ* hybridization, the expression of *ntl* (zebrafish *brachyury*), a

known FGF target gene (Latinkic, B.V. *et al. Genes Dev* 11, 3265-76 (1997)). The expression of *ntl* was greatly expanded within the notochord and the tailbud at the 6-somite stage in BCI-treated embryos (Figure 6d-f). Similarly, BCI treatment from the 1- to 10- somite stage resulted in a marked increase in expression of another FGF target gene, *dusp6,* as shown by the expansion of prospective mid-hindbrain boundary (MHB), rhombomere4 (r4) and the tailbud (Figure 6g & h). The expanded brain structures were confirmed as BCI increased expression of *engrailed3* (*eng3*), which labels MHB, and *krox20,* which demarcates r3 and r5 identity, consistent with previous observations from FGF bead implantation studies (Figure 6i & j)(Maves, L., *et al. Development* 129, 3825-37 (2002)). To further demonstrate that BCI treatment hyperactivated FGF signaling, we measured an increase in the expression of *sef* and *spry4* by semi-quantitative RT-PCR (Figure 6k; n=3 for each gene)(Furthauer, M., *et al. Development* 128, 2175-86 (2001); Tsang, M., *et al. Nat Cell Biol* 4, 165-9 (2002); and Tsang, M. *et al. Development* 131, 2769-79 (2004)). These results confirmed that BCI enhanced FGF signaling in the zebrafish embryo, resulting in the increased transcription of several FGF target genes. We next determined the BCI structural features required to enhance FGF signaling. Two analogs, (*E*)-2-benzylidene-2,3-dihydro-1*H*-inden-1-one (BI) lacking the cyclohexylamino group, and 3-(cyclohexylamino)-2,3-dihydro-1*H*-inden-1-one (ICD) lacking the benzylidene group were synthesized). The cyclohexylamino and benzylidene substituents were both required in enhancing d2EGFP fluorescence, as analogs lacking either group were inactive (Figure 7).

BCI inhibits Dusp6

To determine the mechanism for BCI's activity and to identify a potential target, we probed where this compound acts within the RAS/MAPK pathway. In BCI-treated transgenic embryos, increased d2EGFP expression was restricted to embryonic regions where FGFs are expressed (Fig 1b & c). Furthermore, BCI treatment did not induce d2EGFP expression in the MHB of *Tg(Dusp6:d2EGFP);ace* mutant embryos, which are deficient in Fgf8 signaling (Figure 8d)(Reifers, F. *et al. Development* 125, 2381-95 (1998)). Thus BCI did not enhance FGF signaling in the absence of ligand. We reasoned that BCI could block a feedback attenuator of the FGF pathway, thereby resulting in a net increase in transcription of target genes. To test this model, we determined if BCI could rescue phenotypes generated by ectopic expression of FGF inhibitors, Spry4, Dusp6 and a dominant negative receptor, XFD in zebrafish(Furthauer, M., *et al. Development* 128, 2175-86 (2001) and Tsang, M. *et al. Development* 131, 2769-79 (2004)). Injection of mRNA encoding *dusp6*, *spry4*, or *XFD* into 1-cell stage zebrafish embryos decreased *sef* expression (Figure 8f, 8k, and 8n and Figure 9B). The addition of 5 μM BCI to *dusp6*-injected embryos rescued *sef* expression to control levels or higher (Figure 8g & 8n). In contrast, BCI treatment did not reverse the effects of *spry4* or *XFD* mRNA, suggesting that BCI directly inactivated Dusp6 (Figure 8j and 8n and Figure 9c). To determine if BCI could inhibit other Dusps, we first characterized zebrafish *dusp5* and asked whether it could suppress FGF signaling similar to *dusp6*(Qian, F. *et al. Dev Dyn* 233, 1163-72 (2005) and Sumanas, S., *et al. Blood* 106, 534-41 (2005)). Dusp5 has been shown to dephosphorylate activated ERK (p-ERK) and ectopic

expression of zebrafish *dusp5* inhibited *sef* transcription (Figure 8k and 8n)(Mandl, M., *et al. Mol Cell Biol* 25, 1830-45 (2005)). In contrast to observations with Dusp6 mRNA microinjections, BCI had little or no effect in reversing the phenotype caused by Dusp5 over-expression (Figure 8l & 8n). These observations indicated that BCI was specific for Dusp6. Although both Dusp6 and Dusp5 can dephosphorylate p-ERK and are highly conserved, their catalytic activities are quite different. Dusp6 phosphatase activity is subject to substrate binding and can be catalytically stimulated by ERK interaction (Mandl, M., *et al. Mol Cell Biol* 25, 1830-45 (2005) and Camps, M. *et al. Science* 280, 1262-5 (1998)). This substrate-induced catalytic activity has been described for several members of the Dusp family including Dusp1 (which is sensitive to BCI, as shown below), and Dusp422-24. In contrast, Dusp5 is constitutively activated and substrate binding has little consequence on catalytic rate. Thus the difference we noted with the ability of BCI to rescue Dusp6 but not Dusp5 over-expression *in vivo* suggested that BCI might suppress the activation of Dusp6 associated with substrate binding. Since Dusp6 directly dephosphorylates p-ERK, BCI should restore p-ERK levels in Dusp6 overexpressing cells. We tested this hypothesis in a cell-based chemical complementation assay25,26 in which HeLa cells were transiently transfected with Myc tagged human Dusp6 (Dusp6-Myc), stimulated with 12-*O*-tetradecanoylphorbol-13- acetate (TPA), and immunostained with anti-c-Myc (Figure 10c and d, green) and anti-p- ERK antibodies (Figure 10a and b, red), respectively. Upon TPA treatment, the RAS/MAPK pathway was activated leading to strong p-ERK staining in non-transfected cells, while in cells expressing Dusp6-Myc (Figure 10c), p-ERK staining was abolished (Figure 10a, Dusp6- Myc cells traced in yellow). BCI treatment of Dusp6-Myc transfected cells restored p- ERK levels after TPA addition, suggesting that BCI directly suppressed Dusp6-Myc function (Figure 10b, Dusp6-Myc traced in yellow). In this assay, BCI also inhibited human Dusp1, whose catalytic activity, like Dusp6, is induced by substrate binding (Figure 10e). IC50 values for DUSP6 and DUSP1 inhibition were consistent with hyperactivation of FGF signaling and d2EGFP expression at these concentrations in the zebrafish embryo (Figure 10e). In contrast, treatment with ICD did not block Dusp6 or Dusp1 activity in the chemical complementation assays (Figure 10e). Taken together, we have shown in biological systems BCI specifically inhibited Dusp1 and Dusp6, but not Dusp5.

We next addressed if BCI could directly inhibit Dusp6 activity in an *in vitro* pERK2 dephosphorylation assay. Recombinant Dusp6 completely dephosphorylated pERK2 *in vitro* as determined by immunoblotting with pERK specific antibodies (Figure 10f, Lane 3). Addition of BCI prevented Dusp6-mediated pERK2 dephosphorylation as effectively as the generic tyrosine phosphatase inhibitor sodium orthovanadate (Figure 10f, Lane 4 and 6, respectively). ICD did not block Dusp6 activity supporting the conclusion that BCI directly inhibited Dusp6 (Figure 10f, Lane 5). Since many known small molecule phosphatase inhibitors exhibit low selectivity we determined whether BCI could suppress phosphatase activity from several related phosphatases. BCI did not block Cdc25B (Cell division cycle 25B), PTP1B (Protein Tyrosine Phosphatase 1B) or Dusp3/VHR activity implicating specificity of BCI is limited to a set

of MAP Kinase Phosphatases (Figures 11A-11C). The mean *in vitro* values (μM $n = 3$) for BCI against of recombinant human phosphatases Cdc25B, PTP1B and VHR were > 300 for each phosphatase.

Computational modeling reveals a putative BCI binding site within Dusp6

Crystal structures of several Dusp catalytic domains have been determined (Almo, S.C. *et al. J Struct Funct Genomics* 8, 121-40 (2007); Jeong, D.G. *et al. Proteins* 66, 253-8 (2007); Jeong, D.G. *et al. J Mol Biol* 360, 946-55 (2006); and Stewart, A.E., *et al. Nat Struct Biol* 6, 174-81 (1999)). In each case, the phosphatase domain encompasses a five/six-stranded β-sheet surrounded by five α-helices. These structures enabled us to perform unbiased docking simulations to identify potential BCI binding sites.

BCI was docked onto two different conformations of Dusp6 (MKP3): the low-activity form determined by X-ray crystallography (PDB ID: 1MKP) and the high-activity form obtained by homology modeling using ORCHESTRAR (Tripos, Inc., St. Louis, MO). From cluster analysis of the resulting BCI-bound conformations, we identified a number of potential binding sites on the low-activity form. The most favorable site among them was further assessed by flexible docking using multiple Dusp6 conformations generated by anisotropic network model (ANM) analysis and homology modeling. BCI was predicted to preferentially fit within a crevice between the general acid loop and helix α7, rather than interacting directly with the catalytic residues Asp262, Cys293, or Arg299. At this putative binding site, a close interaction of BCI with the backbone of the general acid loop and the sidechains of Trp264, Asn335 and Phe336 was predicted. Further docking simulations showed that BCI-Dusp1 interactions were comparable to those with Dusp6 rationalizing our observed activity data (Figure 10e).

In further detail,

1. Unbiased docking simulations

BCI was docked onto two different conformations of Dusp6 (MKP3): the low-activity form determined by X-ray crystallography (PDB ID: 1MKP)(Stewart, A.E., *et al. Nat Struct Biol* 6, 174-81 (1999)) and the high-activity form obtained by homology modeling using ORCHESTRAR (Tripos, Inc., St. Louis, MO). We used as templates the structures of Dusp9 (MKP4; PDB ID: 2HXP; 80% sequence identity), Dusp10 (MKP5; PDB ID: 1ZZW; 47% sequence identity), and Dusp5 (VH3; PDB ID: 2G6Z; 44% sequence identity) in the high-activity state (Almo, S.C. *et al. J Struct Funct Genomics* 8, 121-40 (2007); Jeong, D.G. *et al. Proteins* 66, 253-8 (2007); and Jeong, D.G. *et al. J Mol Biol* 360, 946-55 (2006)). For BCI, 400 docking poses (200 per enantiomer) were generated using AutoDock4 for each conformation (see, Huey, R., *et al. Journal of Computational Chemistry* 28, 1145-1152 (2007) and Morris, G.M. *et al. Journal of Computational Chemistry* 19, 1639-1662 (1998)). Genetic algorithm population size was set to 250. Each docking pose was selected based on the energetic evaluation of up to 5×10^6 alternative conformations. The analysis of the resulting poses using an agglomerative clustering scheme revealed the clustering of a subset of binding poses in the vicinity of the active site in both conformations. In the low-activity state, the binding site was a crevice known to close upon catalytic activation of the enzyme. In the

high-activity state this crevice is not accessible. Instead, a relatively more hydrophobic patch in the neighborhood of the active site was predicted to serve as an alternative binding site for the inhibitor (see, Lazo, J.S. *et al. J Pharmacol Exp Ther* 322, 940-7 (2007)). Based on these observations two potential inhibition mechanisms were hypothesized:

(i) BCI binds the low-activity form of Dusp6 and restricts the mobility of the general acid loop so as to prevent ERK2 from inducing the conformational changes that lead to Dusp6 catalytic activation. This restricts ERK2 dephosphorylation to a basal catalytic rate.

(ii) BCI binds the ERK-actived Dusp6, and prevents ERK2 from optimally orienting itself, which leads to the inhibition of ERK2 dephosphorylation. In either case, BCI was not expected to prevent Dusp6-ERK2 complex formation due to the large surface area of interaction distributed over two domains of Dusp68.

2. Flexible docking

Toward an assessment of the more likely inhibition mechanism among those hypothesized above, we further explored the binding properties of BCI by allowing the protein to undergo structural fluctuations in the neighborhood of the two above-defined states. Backbone flexibility was deduced from normal mode analysis and homology modeling calculations. Conformations accessible near the basal-activity state were sampled by using the anisotropic network model (ANM) in combination with all-atom energy minimization (Atilgan, A.R. *et al. Biophys J* 80, 505-15 (2001)). Third, fourth, and fifth ANM slow modes were found to set in motion the catalytic Asp262 close to the catalytic cavity (Eyal, E., *et al. Bioinformatics* 22, 2619-27 (2006)). The general acid loop was also observed to have a tendency to move towards the catalytic cavity in 10 ns long unbiased molecular dynamics simulations, in line with AMN calculations. NAMD software and the Charmm force field were used for energy minimization (MacKerell Jr., *et al. J. Phys. Chem.* 102, 3586-3616 (1998) and Phillips, J.C. *et al. J Comput Chem* 26, 1781-802 (2005)). For each α-carbon, harmonic restraints with a force constant of 40 kcal/mole/Å2 were defined to drive the motions along the selected ANM modes at steps of size < 0.2 Å, similar to recently introduced ANM-steered simulations (Isin, B., *et al. Biophys J* 95, 789-803 (2008)). A total of twenty conformations were sampled along the selected modes by jointly optimizing backbone and side-chain conformations (Lovell, S.C., *et al. Proteins* 40, 389-408 (2000)). As for the high-activity state, multiple models generated with MODELLER were used as targets (Jones, G., Willett, *et al. J Mol Biol* 267, 727-48 (1997)). Asp262, Trp264, and Asn335 side chains were allowed to sample rotameric states from Penultimate library (Lovell, S.C., *et al. Proteins* 40, 389-408 (2000)).

At least 1000 docking poses for the basal and activated state were generated using GOLD and cluster analysis was performed(Jones, G., Willett, *et al. J Mol Biol* 267, 727-48 (1997)). Docking poses were scored using GoldScore, which is a weighted sum of van der Waals energy and hydrogen bond energy that implicitly accounts for charged interactions (Jones, G., *et al. J Mol Biol* 245, 45-53 (1995)). The

most populated and energetically favorable clusters were examined to identify the most favorable docking solution. The most favorable cluster of BCI docking poses was located in the low-activity conformation. The corresponding GoldScore averaged over all binding poses for this cluster was found to be 47.2 ± 2.1, in favor of the hypothesis (i). Finally, as a further verification, docking simulations were performed to compare the binding properties of BCI against Dusp5, Dusp1 and Dusp6. BCI was docked onto to the crystal structure of Dusp5 (PDB ID: 2G6Z) and a model of Dusp1 based on Dusp6 structure using the same procedure as described above for Dusp6. Docking to the Dusp5 crystal structure yielded much lower docking scores (27.9 ± 1.4) due to lack of the crevice observed in Dusp6, explaining lack of activity against this constitutively active homolog. Docking of BCI to the Dusp1 model resulted in comparable interaction but lower Goldscores (37.4 ± 2.9). The Dusp6 movies (not shown) were generated using energy minimization with harmonic constraints based on ANM modes, implemented following the procedure described in Isin, B., *et al.* (*Biophys J* 95, 789-803 (2008)). Movie 1, which shows intrinsic flexibility of the general acid loop was generated using 3rd, 4th, and 5th slow modes. Movie 2, which shows the catalytic activation of Dusp6 was generated using 5% of the entire spectrum of modes in the low frequency regime.

In the zebrafish microinjection assays, BCI inhibited ectopic expression of *dusp6* but not *dusp5*, exhibiting specificity toward certain members of this phosphatase family (Figure 8). To understand how BCI can block Dusp6 but not Dusp5, we compared the two phosphatase crystal structures. Structural superposition of Dusp5 and Dusp6 displayed that the particular crevice in Dusp6 that accommodates BCI binding that is not accessible in Dusp5. As a result, docking of BCI onto the same region of Dusp5 phosphatase domain resulted in energetically less favorable interactions. The relative positions of Asp262 and Asp232 in the respective phosphatases Dusp6 and Dusp5 differ by 5Å after optimal superposition of the two structures, suggesting that their basal activities are determined by the relative location of these catalytic residues (Jeong, D.G. *et al. Proteins* 66, 253-8 (2007)). It was postulated that substrate binding to Dusp6 induces a conformational shift that reorients Asp262 towards the phosphatase loop, thereby creating a high activity enzyme (Owens, D.M. *et al. Oncogene* 26, 3203-13 (2007)). In support of this model, mutation of Asp262 to asparagine did not abolish basal phosphatase activity, but suppressed catalytic activation upon ERK binding (Stewart, A.E., *et al. Nat Struct Biol* 6, 174-81 (1999)). To further understand BCI action on Dusp6 mechanistically, we explored Dusp6 dynamics by particularly focusing on the ANM modes that induce conformational changes at the general acid loop. Our analysis showed that Dusp6 possesses an intrinsic, structure induced tendency to suitably reorient its general acid loop to position Asp262 closer to the phosphatase loop. Therefore, without any intent to be bound by this theory, we proposed that BCI binding to the accessible crevice in the low-activity form effectively blocks the flexibility of this loop, thereby preventing the interaction of Asp262 with the other catalytic residues. Such constraints on functional motions are likely to inhibit Dusp6 activation induced by ERK binding.

BCI is an allosteric inhibitor of Dusp6

We measured the dephosphorylation of a small molecule phosphatase substrate, 3-*O*-methylfluorescein phosphate (OMFP), by Dusp6 in the presence or absence of ERK2. Docking simulations predicted that BCI and OMFP could simultaneously bind within the phosphatase active site with OMFP interfacing with the core catalytic residues. This suggests that BCI would not block basal Dusp6 phosphatase activity toward OMFP. Indeed, at a concentration that inhibited ERK dephosphorylation *in vitro* (100 μM), BCI did not inhibit basal Dusp6 activity (Figure 12a). Addition of ERK2 protein stimulated Dusp6 dephosphorylation of OMFP three-fold and this enhancement was significantly inhibited in the presence of BCI (57% inhibition) (Figure 13). Increasing the ratio of ERK2 to Dusp6 (10:1) in the activation assay resulted in a 7-fold enhancement that was also suppressed by the addition of BCI (30% inhibition) (Figure 12b). These data support the modeling predictions that BCI is a specific allosteric inhibitor of Dusp6 that prevents the catalytic stimulation of phosphatase activity induced by substrate binding.

The role of Dusp6 and FGF in regulating heart size

The identification of a small molecule that blocks the biologically relevant activity of Dusp6 and Dusp1 allowed us to probe the requirement for these enzymes in later developmental processes. Given that BCI could potentially block related members of the Dusp family, we examined the expression of other *dusps* in zebrafish. Detailed expression analyses of several *dusps* have been described and include *dusp4*, *dusp1*, *dusp7*, *dusp5*, and *dusp22a* (Qian, F. *et al. Dev Dyn* 233, 1163-72 (2005); Sumanas, S., *et al. Blood* 106, 534-41 (2005); Brown, J.L. *et al. Proc Natl Acad Sci U S A* 105, 12337-42 (2008); Kudoh, T. *et al. Genome Res* 11, 1979-87 (2001); and Thisse, B. *et al.* Fast Release Clones: A High Throughput Expression Analysis. ZFIN Direct Data Submission (zfin.org) (2004)). Of these only Dusp6 functions as a feedback regulator of FGF/MAPK/ERK signaling and is expressed within the anterior lateral plate mesoderm, supporting the idea that this phosphatase plays a role in heart development. In early embryogenesis, Dusp6 is an important regulator of FGF signaling; knock-down with antisense morpholinos results in embryo polarity defects, which precludes the study of Dusp6's role in later development (Tsang, M. *et al. Development* 131, 2769-79 (2004)). In contrast, small molecules permit the analysis at later stages of development due to rapid and transient perturbation of their biological targets. Using BCI as a chemical probe, we asked how inhibiting Dusp6 activity would alter patterning and formation of the heart. The zebrafish heart develops from a small group of cardiac progenitor cells that can be identified by 5hpf within the mesodermal layer of the blastula stage embryo. During gastrulation, cardiac progenitor cells undergo cellular migration to form two bilateral populations known as the anterior lateral plate mesoderm (ALPM) located just behind the MHB, and begin to express the transcription factors *nkx2.5* and *gata4*. Studies have described a role for Fgf8 in zebrafish heart development. In embryos harboring an fgf8 mutation, both atria and ventricular cells are reduced (Marques, S.R., *et al. Dev Biol* 321, 397-406 (2008) and Reifers, F., *et al. Development* 127, 225-35 (2000)). In agreement with the notion that FGF signaling plays a role in stipulating heart size, ectopic expression of a constitutively activated FGF receptor (Fgfr1) during somitogenesis stages expanded cardiac

tissue (Marques, S.R., *et al. Dev Biol* 321, 397-406 (2008)). Therefore we used BCI to test if Dusp6 limits FGF signaling and restricts cardiac progenitors and heart organ size. In BCI-treated embryos a caudal expansion of *gata4* in the ALPM was observed (compare Figure 14a & a' to 14b & b'; 81%, n=16). The *gata4* caudal expansion of the ALPM corresponds to where cardiac progenitors are situated at the 10-somite stage.

Examination of *nkx2.5* expression in BCI-treated embryos showed expanded cardiac progenitor pools as compared to DMSO-treated embryos, confirming a specific effect on heart precursors (compare Figure 14d to 15d; 91%, n=11). While we noted an expansion of cardiac progenitors, it was not clear if this event was at the expense of other lineages. Recent studies have shown that there exists a repressive interaction between the vascular and hematopoietic precursors on cardiomyocyte progenitors that determine heart organ size (Schoenebeck, J.J., *et al. Dev Cell* 13, 254-67 (2007)). We analyzed expression of *scl/tal1*, a gene that is expressed in endothelial and blood lineages located within the rostral domain of the ALPM in BCItreated embryos from the 1-somite stage. Inhibition of Dusp6 resulted in a marked reduction in *scl* expression, suggesting that activation of FGF signaling expanded cardiac tissue at the expense of blood or endothelial progenitors (compare Figure 14f to 14e; 93%, n=15). Likewise, *etsrp*, a marker for vascular fate was also reduced in BCI-treated embryos (data not shown). The loss of endothelial and hematopoietic lineages was coupled with the concomitant expansion of cardiac *hand2* expression at the 10-somite stage (Figure 14f; 32%, n=19). This surplus of cardiac progenitors was also noted at the 18-somite stage by an increase in cells positive for *cardiac myosin light chain 2* (*cmlc2*), which specifically labels differentiated cardiomyocytes (Figure 14h; 81% n=16). To test whether the expansion of cardiac progenitors resulted in an increase in heart tissue, we analyzed treated embryos at larval stage. Embryos were treated at 40% epiboly, with BCI or DMSO, followed by compound washout the next day and further incubation until the embryos reached 56hpf. In BCI-treated larvae, we noted a marked expansion in cardiac tissue (Figure 14j & o). To define the critical period as to when Dusp6 activity limits heart organ size, we treated embryos at the 1- and 8-somite stages. We observed larger hearts at both time points, however the frequency was reduced in embryos treated at the later stage (Figure 14o). *In situ* analysis with probes for *ventricular myosin heavy chain* (*vmhc*) and *cmlc2* confirmed that treated embryos exhibited enlarged hearts (Figure 14l & n, and Figure 15). Expansion was particularly notable for ventricular tissue, known to be sensitive to Fgf8 signaling (Figure 14l)(Marques, S.R., *et al. Dev Biol* 321, 397-406 (2008) and Reifers, F., *et al. Development* 127, 225-35 (2000)). These results indicate that inhibition of Dusp6 by a small molecule inhibitor can induce an expansion of myocardial progenitors that ultimately increase heart size.

Discussion

The zebrafish embryo offers distinct advantages over traditional *in vitro* and cell-based chemical screens. With the generation of transgenic FGF reporter lines, it is possible to screen for novel compounds that modulate this pathway *in vivo*. In addition, live embryo screens allow for the elimination of toxic compounds and molecules that evoke non-specific effects on embryo differentiation. From a modest screen

of approximately 5000 compounds, we identified BCI, a small molecule that enhanced FGF signaling. Subsequent *in vitro* phosphatase assays and docking simulations provided strong evidence that BCI suppressed the ERK-induced activation of Dusp6. The identification of BCI allowed us to directly probe the role of Dusp6 in heart formation during a critical period when cardiac specific transcription factors begin to be expressed and are consistent with studies when global activation of FGF signaling resulted in increased cardiac progenitors. Treatment with BCI resulted in the expansion of the cardiac field at the expense of endothelial lineages. The increase in cardiac progenitors resulted in enlarged hearts, suggesting that FGF signaling must be tightly regulated during this period to allow for proper cardiac morphogenesis to occur. The role for Dusp6 in controlling heart organ size is likely conserved with other vertebrates as disruption of Dusp6 was recently found to cause enlarged hearts (Maillet, M. *et al. J Biol Chem* 283, 31246-55 (2008)).

Previous high-throughput screens for Dusp6 and Dusp1 inhibitors involved *in vitro* assays with artificial substrates. Because these assays do not faithfully recapitulate phosphatase activity in a biological context, no specific Dusp6 inhibitors with *in vivo* activity have been identified (Ducruet, A.P., *et al. Annu Rev Pharmacol Toxicol* 45, 725-50 (2005)). The phosphatase catalytic site is highly conserved across all tyrosine phosphatases and crystal structures have revealed shallow catalytic pockets. These structural features have further hampered the identification of specific small molecule phosphatase inhibitors (Bakan, A., *et al. Curr Med Chem* 15, 2536-44 (2008)). Small molecules targeting Dusp1 identified from *in vitro* screens have exhibited promiscuous activity or lack potency (Lazo, J.S. *et al. Bioorg Med Chem* **14**, 5643-50 (2006)). However, with the identification of a novel allosteric inhibitor and our understanding of its mechanism of action, it is possible to design new molecules based on BCI to block substrateinduced Dusp function. This offers highly specific compounds to probe the role of Dusps in development, and potentially provide novel compounds for treatment of diseases that are dependent on FGF signaling such as wound repair and regeneration.

Example 2 –Synthesis of BCI

BCI was synthesized by aldol condensation of 2,3-dihydro-1*H*-inden-1-one with benzaldehyde, bromination and SN2 addition of cyclohexylamine for subsequent studies. (*E*)-2-Benzylidene-2,3-dihydro-1*H*-inden-1-one (BI) and 3-(cyclohexylamino)- 2,3-dihydro-1*H*-inden-1-one (ICD) were prepared by bromination of 2,3-dihydro-1*H* inden-1-one and displacement of bromide with cyclohexylamine. All reactions were conducted in oven-dried glassware under a dry atmosphere. Starting materials, reagents and anhydrous solvents were purchased from commercial suppliers (Sigma-Aldrich and Fisher). Reactions were monitored by TLC on EM Science pre-coated silica gel 60 F254 plates, 250 μm layer thickness. Flash chromatography was performed over silica gel 60, 230-400 mesh. Low resolution mass spectra (MS) were obtained in electron ionization (EI) mode on a Hewlett Packard 5971 mass selective detector coupled to a Hewlett Packard 5890 Series II gas chromatograph equipped with a 30 m 5% phenyl methylsilicone capillary column from Supelco. High resolution mass spectra (HRMS) were obtained with an Applied Biosystems 4700 MALDI-TOF instrument using α-cyano-4-hydroxycinnamic acid as the matrix. Melting

points were determined on a Fisher-Johns open stage apparatus and are uncorrected. ^{1}H and ^{13}C NMR spectra were recorded on a Varian Mercury spectrometer at 400 and 100 MHz, respectively, or a Bruker Avance spectrometer at 600 and 150 MHz, respectively. NMR chemical shifts were referenced to the residual $CHCl_3$ signal (7.26 ppm downfield from Me4Si) and ^{13}C NMR chemical shifts to the solvent CDCl3 signal (77.00 ppm downfield from Me4Si), respectively.

Example 3: (*E*)-2-Benzylidene-2,3-dihydro-*1H*-inden-1-one

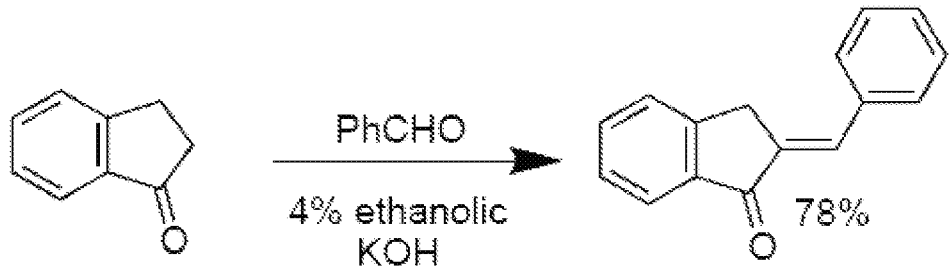

(*E*)-2-Benzylidene-2,3-dihydro-*1H*-inden-1-one was synthesized as described by Hassner and Cromwell (*J Am Soc Chem* 80, 893-900 (1958). An ice bath-cooled mixture of 2,3-dihydro-1*H*-indan-1-one (2.0 g, 15.1 mmol) and benzaldehyde (1.6 g, 15.1 mmol) was treated dropwise with 4% ethanolic KOH (*w/v*) with stirring until precipitation ceased. After an additional 1 h of stirring at room temperature, the precipitate was collected by filtration, washed with cold H_2O, then recrystallized from MeOH-H_2O to give the title compound as straw-colored crystals (2.6 g, 78% yield): M.p. 109-110°C; ^{1}H NMR (400 MHz, $CDCl_3$): δ 4.07 (s, 2H), 7.34–7.78 (m, 9H), 7.94 (d, ^{1}H, *J*=7.6 Hz); ^{13}C NMR (100 MHz, $CDCl_3$): δ 33.3, 125.1, 128.0, 129.1, 130.5, 131.6, 132.6, 134.8, 136.4, 137.3, 139.6, 151.4, 194.3; MS (EI) *m/z* (relative intensity): 220 ($M^{+\bullet}$, 55), 219 (M-1, 100). HRMS (MALDI-TOF) calc'd for *m/z* 221.0966 $[M+H]^+$, found 221.0970. CAS Registry No: [17434-21-8].

Example 4: (*Z*)-2-Benzylidene-3-bromo-2,3-dihydro-1*H*-inden-1-one

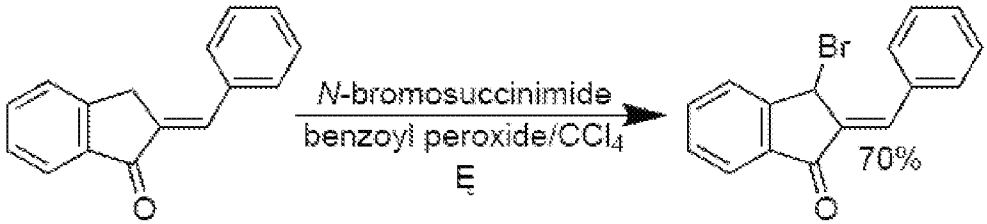

(*Z*)-2-Benzylidene-3-bromo-2,3-dihydro-1*H*-inden-1-one was generated as described by Pearson et al. (*J Org Chem* 27, 3038-3044 (1962)). Briefly, (E)-2-Benzylidene-2,3-dihydro-1H-inden-1-one (1.0 g, 4.5 mmol), N-bromosuccinimide (0.8 g, 4.5 mmol) and benzoyl peroxide (61 mg, 0.25 mmol) were dissolved in 15 mL of CCl_4. The mixture stirred and heated to reflux for 1h under a N_2 atmosphere. The mixture was cooled to r.t. and stirred an additional 1h. After filtration and concentration from solvent under vacuum, the resulting orange solid was recrystallized three times from CCl_4 to give the title compound as a straw-colored solid (0.94 g, 70% yield): M.p. 118-119°C; 1H NMR (400 MHz, $CDCl_3$): δ 6.33 (s, ^{1}H, C3-H), 7.19-7.85 (m, 10H, 9 aromatic, 1 vinyl); ^{13}C NMR (100 MHz, $CDCl_3$): δ 39.9, 127.4, 127.8, 128.4, 128.6, 128.7, 129.4, 134.1, 134.9, 135.6, 139.6, 141.9, 149.4, 192.8; MS (EI) *m/z* (relative intensity): 296 ([^{77}Br]$M^{+\bullet}$, 14); HRMS (MALDI-TOF) calc'd for *m/z* 297.0102 [[^{77}Br]M+H]$^+$, found 297.0096. CAS Registry No: [5387-50-8].

Example 5: 3-Bromo-2,3-dihydro-1*H*-inden-1-one

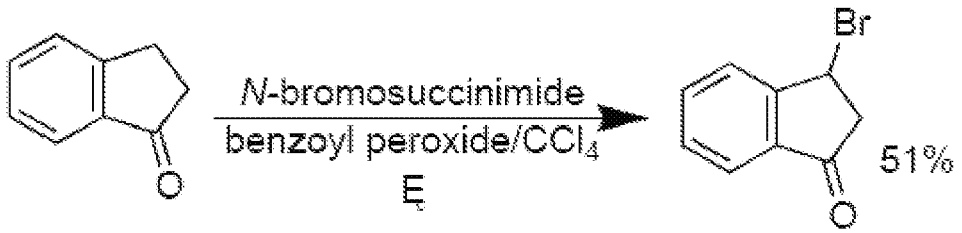

3-Bromo-2,3-dihydro-1*H*-inden-1-one was generated as described by Treibs and Schroth 34. 2,3-Dihydro-1*H*-indan-1-one (528 mg, 4 mmol), *N*-bromosuccinimide (684 mg, 4 mmol) and benzoyl peroxide (30 mg, 0.12 mmol) were dissolved in CCl_4 (10 mL) and heated to reflux for 1h under an N_2 atmosphere. After cooling, succinimide was removed by filtration and the filtrate concentrated under high vacuum to yield the title compound as a straw-colored oil of > 99% purity as seen by GC-MS and NMR that was used without further purification (428 mg, 51% yield). ^{1}H NMR (600 MHz, $CDCl_3$): δ 3.064 (dd, 1H, *J*=19.7, *J*=2.3 Hz, CH_2), 3.370 (dd, 1H, *J*=19.7Hz, *J*=7.2Hz, CH_2) 5.609 (dd, 1H, *J*=7.2Hz, *J*=2.6Hz, C3-H), 7.468-7.520 (m, 1H), 7.702-7.775 (m, 3H); ^{13}C NMR (150 MHz, $CDCl_3$): δ 40.28, 50.30, 127.29, 128.81, 128.86, 133.72, 138.00, 204.55; MS (EI) *m/z* (relative intensity): 208 ([77Br]$M^{+\bullet}$, 22). CAS Registry No: [40774-41-2].

Example 6: 3-(Cyclohexylamino)-2,3-dihydro-1*H*-inden-1-one (ICD)

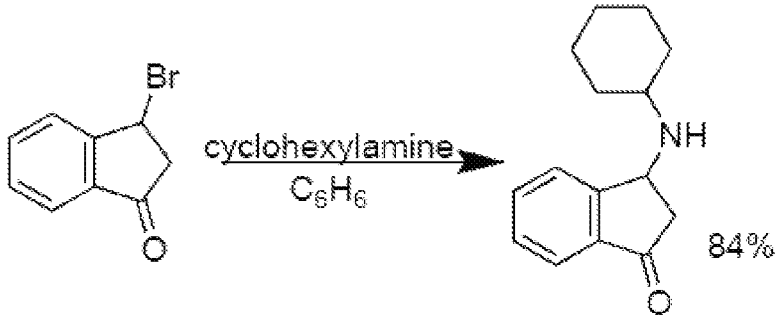

3-Bromo-2,3-dihydro-1*H*-inden-1-one (100 mg, 475 μmol) and cyclohexylamine (94 mg, 951 μmol) were dissolved in 2 mL of dry benzene and stirred under N_2 until precipitation ceased (~15 min). The cyclohexylamine•HBr was removed by filtration. The filtrate was applied to a flash SiO_2 column that was developed with 8:1 hexanes-EtOAc to give the title compound as a clear oil (91 mg, 84% yield).

Example 7: General procedure for the synthesis of 2 -benzylideneindan-1-ones

Corresponding indanone (20 mmol) and corresponding benzaldehyde (20 mmol) were dissolved in methanol (50 mL). Potassium hydroxide (280 mg, 5 mmol) was added in one portion and reaction mixture was stirred at rt for 24 h. Most of solvent was removed in vacuum, and reaction was quenched with water 100 mL. Product was extracted by dichloromethane (3 × 100 mL), combined organic fractions were dried over $MgSO_4$, filtered and concentrated.

Example 8: (3-Bromo-2-(4-chlorobenzylidene)indan-1-one) 14a:

2-(4-chlorobenzylidene)indan-1-one (2.44g, 9.58 mmol) was dissolved in 35 mL of CCl_4. *N*-bromosuccinimide (1.685 g, 9.58 mmol) and benzoyl peroxide (122 mg, 0.52 mmol) were added in one portion. The solution was then stirred under reflux for one hour and then filtered once cooled to room temperature. The precipitate was separated using flash column chromatography (15:1 Hexanes/EtOAc) provided **14a** as white crystals.

Example 9: (4-(1-Bromo-3-oxoindan-2-ylidenemethyl)benzonitrile) 15a:

4-(1-Oxoindan-2-ylidenemethyl)benzonitrile (2.18 g, 8.9 mmol) was dissolved in carbon tetrachloride (40 mL). *N*-bromosuccinimide (1.58 g, 8.9 mmol) and benzoyl peroxide (100 mg) were added in one portion. Reaction mixture was reflux for 9 h, cooled down; precipitate was filtered off and washed with diethyl ether (10 × 30 mL) for removal of *N*-hydroxysuccinimide. Precipitate was dried under vacuum, provided pure **15a**.

Example 10: General procedure for the synthesis of compounds 3-16 and 19-32

Corresponding 2-benzylidene-3-bromoindan-1-one **2** (299 mg, 1 mmol) or substituted analog was dissolved in benzene (10 mL). Corresponding amine (2 mmol) was added in one portion and reaction mixture was stirred for 24 h. Solvent was removed in vacuum and product was isolated by column chromatography (silica0.

Example 11: Synthesis of 2-Benzylidene-3-cycloheptylaminoindan-1-one (5)

2-Benzylidene-3-bromoindan-1-one **2** (299 mg, 1 mmol) was dissolved in benzene (10 mL). Cycloheptylamine (255 µL, 2 mmol) was added and reaction mixture was stirred for 24 h. Solvent was removed in vacuum and **5** (271 mg, 82 %) was isolated as yellow crystals by column chromatography (Hexanes/EtOAc 9:1) followed by crystallization from dichloromethane with pentane.

Example 12: Synthesis of (2-Benzylidene-3-cyclohexylaminoindan-1-ol) 18

2-Benzylidene-3-cyclohexylamino-indan-1-one (**3**, **BCI**) (317 mg, 1 mmol) was dissolved in dry THF (15 mL) under nitrogen. Solution of $LiAlH_4$ (76 mg, 2 mmol) in dry THF (10 mL) was added dropwise at 0 °C. Solution was stirred overnight and quenched with 100 µL of water followed by 100 µL of 15 % NaOH followed by 300 µL of water. Precipitate was filtered off and washed with ether (3 × 30 mL). Combined liquid was evaporated in vacuum, and residue was separated by column chromatography on silica (DCM-MeOH-NH_4OH 100:1:0.5).

Example 13: Synthesis of (5-(2-Oxohexahydrothieno[3,4-*d*]imidazol-4-yl)-pentanoic acid (4-amino-cyclohexyl)amide) 19b

1,4-Diaminocyclohexane (37.6 mg, 0.33 mmol) was dissolved in dry DMF (3 mL) under nitrogen. Solution of NHS-Biotin (102.3 mg, 0.3 mmol) in dry DMF (3 mL) was added to stirred solution of diamine over a 15 min period. Reaction mixture was stirred for 16 h at ambient temperature. Dilution of reaction mixture with dry Et_2O (50 mL) produced white precipitate. Precipitated **19b** was filtered, washed with EtOAc (3 × 20 mL) for removing of NHS and dried in high vacuum.

Example 14: Characterization of compounds

Table 2 contains characterization details for the indicated compounds.

Table 2. Characterization of BCI analogs

Compound	Yield	Rf	Mp (°C)	**^{1}H NMR** ($CDCl_3$, 600 MHz): δ	**^{13}C NMR** ($CDCl_3$, 150 MHz): δ	HPLC/MS	HRMS
4 **VNK-I-16**	91 %	0.20 Hex/EA 3 : 1	Yellow oil	0.98-1.07 (m, 1H), 1.22-1.64 (m, 7H), 1.79 (br.s, 1H, NH), 2.94 (quintet, *J* = 6.6 Hz, 1H), 5.34 (s, 1H, C*H*N), 7.39-7.43 (m, 1H), 7.47 (t, *J* = 7.2 Hz, 2H), 7.50 (d, *J* = 7.2 Hz, 1H), 7.66 (t, *J* = 7.8 Hz, 1H), 7.71 (d, *J* = 7.8 Hz, 1	23.43, 23.69, 33.24, 34.40, 55.36, 56.38, 124.04, 126.23, 128.61, 128.65, 129.69, 131.34, 134.47, 134.72, 135.93, 137.57, 138.34, 152.55, 193.54	VNK-164AAA > 95 % purity	Calcd. 304.1701 Observed 304.1699
5 **VNK-I-165**	82 %	0.25 Hex/EA 3 : 1	Yellow crystals 90-92	1.14-1.74 (m, 13H), 2.68-2.74 (m, 1H), 5.35 (s, 1H), 7.40-7.44 (m, 1H), 7.48 (t, *J* = 7.2 Hz, 2H), 7.49-7.52 (m, 1H), 7.65-7.69 (m, 2H), 7.76 (s, 1H), 7.93 (d, *J* = 7.2 Hz, 1H), 7.96 (d, *J* = 7.8 Hz, 2H).	23.77, 23.90, 28.52, 28.68, 34.24, 36.52, 54.25, 55.47, 124.21, 126.26, 128.64, 128.68, 129.75, 131.50, 134.50, 134.84, 135.93, 137.44, 138.44, 152.70, 193.71.	VNK-165AAA > 95 % purity	Calcd. 332.2014 Observed 332.2007
6 **VNK-I-149**	69 %	0.25 Hex/EA 3 : 1	Orange crystals 153-155	3.92 (br.s, 1H, NH), 6.01 (s, 1H), 6.78 (d, *J* = 8.4 Hz, 2H), 6.81 (t, *J* = 7.8 Hz, 1H), 7.24 (t, *J* = 7.8 Hz, 2H), 7.29-7.35 (m, 3H), 7.48 (t, *J* = 7.8 Hz, 1H), 7.54 (t, *J* = 7.8 Hz, 1H), 7.63 (d, *J* = 7.8 Hz, 1H), 7.68 (d, *J* = 6.6 Hz, 2H), 7.80 (d, *J* = 1.2 Hz, 1H), 7.90 (d, *J* = 7.2 Hz, 1H)	53.50, 113.64, 118.53, 124.02, 125.41, 128.71, 129.15, 129.59, 130.15, 132.07, 133.68, 135.33, 136.32, 136.78, 137.16, 146.93, 152.68, 192.81	VNK-149 > 95 % purity	Calcd. 312.1388 Observed 312.1390
7 **VNK-I-147**	81 %	0.55 Hex/EA 1 : 1	Slightly yellow crystals 140-142	1.34-1.39 (m, 2H), 1.46-1.54 (m, 4H), 2.43 (br.s, 2H), 2.66-2.73 (m, 2H), 5.04 (d, *J* = 0.6 Hz, 1H, CHN), 7.39-7.43 (m, 1H), 7.45-7.52 (m, 3H), 7.61-7.67 (m, 2H), 7.74 (d, *J* = 1.2 Hz, 1H), 7.94 (d, *J* = 7.8 Hz, 1H), 8.08 (dd, *J* = 7.8 Hz, *J* = 1.2 Hz, 2H)	24.69 (CH_2), 26.49 (CH_2), 50.15 (CH_2N), 65.04 (CHN), 124.17 (CH), 126.81 (CH), 128.39 (CH), 128.66 (CH),129.69 (CH), 132.63 (CH), 133.96 (CH), 135.12 (C-q), 136.86 (CH), 137.83 (C-q),138.37 (C-q), 149.68 (C-q), 193.65 (C=O)	VNK-147 > 95 % purity	Calcd. 304.1704 Observed 304.1700

8 **VNK-I-53**	89 %	0.4 Hex/EA 1 : 1	Yellow crystals 179-181	**VNK-I-053H**: 0.89 (quin.d, *J* = 12.6 Hz, *J* = 3.0 Hz, 2H), 1.05 (quin., *J* = 13.2 Hz, 2H), 1.24-1.31 (m, 1H), 1.40 (br.s., 9H), 1.43 (s, 1H), 1.58 (d, *J* = 12.6 Hz, 1H), 1.76 (dt, *J* = 12.0 Hz, *J* = 2.4 Hz, 1H), 1.83 (d, *J* = 12.0 Hz, 1H), 2.30 (d, *J* = 4.8 Hz, 1H), 3.26 (br.s., 1H), 4.34 (br.s., 1H), 5.35 (d, *J* = 1.2 Hz, 1H), 7.38-7.50 (m, 4H), 7.62-7.67 (m, 2H), 7.75 (d, *J* = 1.2 Hz, 1H), 7.85 (d, *J* = 7.2 Hz, 1H), 7.89 (d, *J* = 7.2 Hz, 1H)	**VNK-I-053CC:** 28.39, 31.80, 31.91, 32.48, 33.29, 49.15, 51.81, 55.45, 79.06, 124.10, 126.11, 128.72, 129.86, 131.31, 134.68, 134.74, 136.11, 137.40, 138.09, 152.78, 155.16, 193.52	VNK-053 > 95 % purity	Calcd. 433.2491, Observed 433.2491`
9 **VNK-I-148**	81 %	0.45 Hex/EA 1 : 1	Yellow crystals 138-140	2.47 (br.s, 2H), 2.73 (br.s, 2H), 3.62 (t, *J* = 4.5 Hz, 4H, *CH_2O*), 5.08 (d, *J* = 0.6 Hz, 1H, *CH*N), 7.42-7.50 (m, 3H), 7.51-7.55 (m, 1H), 7.64 (d, *J* = 3.0 Hz, 2H), 7.76 (d, *J* = 1.2 Hz, 1H), 7.93 (d, *J* = 7.2 Hz, 1H), 7.99 (d, *J* = 7.2 Hz, 2H)	49.05 (CH_2N), 64.41 (CHN), 67.29 (CH_2O), 124.31 (CH), 126.86 (CH), 128.49 (CH), 129.08 (CH), 129.96 (CH), 132.36 (CH), 134.28 (CH), 134.82 (C-q), 136.64 (C-q), 137.28 (CH), 138.38 (C-q), 148.71 (C-q), 193.17 (C=O)	VNK-148 > 95 % purity	Calcd. 304.1338 Observed 304.1447
10 **VNK-I-177**	87 %	0.30 Hex/EA 3 : 1	Slightly yellow crystals 143-145	2.50-2.62 (m, 4H), 2.73-2.85 (m, 2H), 2.95-3.05 (m, 2H), 5.09 (d, *J* = 1.2 Hz, 1H, C*H*N), 7.44 (d, *J* = 6.6 Hz, 1H), 7.47 (t, *J* = 7.2 Hz, 2H), 7.52 (ddd, *J* = 8.4 Hz, *J* = 6.0 Hz, *J* = 3.0 Hz, 1H), 7.65-7.68 (m, 2H), 7.77 (d, *J* = 1.8 Hz, 1H), 7.96 (t, *J* = 8.4 Hz, 2H), 7.97 (s, 1H)	28.41, 51.71, 65.80, 124.33, 126.65, 128.42, 129.01, 129.96, 132.41, 134.40, 134.66, 136.69, 137.30, 138.24, 149.04, 193.16	VNK-177 > 95 % purity	Calcd. 322.1266 Observed 322.1269
11 **VNK-I-187**	42 %	0.20 DCM	Yellow crystals	2.20-2.70, 4.97 (s, 1H, CHN), 7.28-7.33 (m, 3H), 7.42 (d, *J* = 7.8 Hz, 1H), 7.50 (t, *J* = 7.2	64.18, 124.20, 126.83, 128.35, 128.84, 129.74, 132.41, 134.18, 134.83, 137.09,		Calcd. 305.1654

			245-248	Hz, 1H), 7.55 (t, *J* = 7.2 Hz, 1H), 7.74 (d, *J* = 0.6 Hz, 1H), 7.91 (dd, *J* = 6.6 Hz, *J* = 1.8 Hz, 2H), 7.94 (d, *J* = 7.2 Hz, 1H)	137.17, 138.24, 149.08, 193.39		Observed 305.1652
12 VNK-I-178	92 %	0.55 DCM/ MeOH/ NH_4OH 90: 10: 1	Yellow oil	2.21 (s, 3H, CH_3), 2.25-3.00 (m, 8H), 5.08 (s, 1H, C*H*N), 7.42 (t, *J* = 7.2 Hz, 1H), 7.46 (t, *J* = 7.2 Hz, 2H), 7.48 (t, *J* = 7.2 Hz, 1H), 7.59 (td, *J* = 7.2 Hz, *J* = 1.2 Hz, 1H), 7.65 (d, *J* = 7.8 Hz, 1H), 7.74 (d, *J* = 1.2 Hz, 1H), 7.92 (d, *J* = 7.2 Hz, 1H), 8.01 (d, *J* = 1.2 Hz, 2H)	45.99, 55.42, 64.12, 124.22, 126.95, 128.45, 128.92, 129.80, 132.49, 134.14, 134.96, 137.09, 137.20, 138.29, 149.04, 193.39	VNK-178 > 95 % purity	Calcd. 319.1810 Observed 319.1800
13 VNK-I-179	86 %	0.20 EtOAc	Yellow oil	1.98 (s, 3H, CH_3), 2.23 (t, *J* = 7.8 Hz, 1H), 2.57-2.62 (m, 1H), 2.65-2.69 (m, 1H), 2.77 (t, *J* = 7.8 Hz, 1H), 3.20 (t, *J* = 9.0 Hz, 1H), 3.29 (t, *J* = 9.0 Hz, 1H), 3.33-3.39 (m, 1H), 3.81 (d, *J* = 10.2 Hz, 1H), 5.16 (s, 1H, CHN), 7.41 (t, *J* = 6.6 Hz, 1H), 7.45 (t, *J* = 7.2 Hz, 2H), 7.50 (t, *J* = 7.2 Hz, 1H), 7.57 (d, *J* = 7.2 Hz, 1H), 7.63 (t, *J* = 7.2 Hz, 1H), 7.76 (br.s, 1H), 7.91 (d, *J* = 7.8 Hz, 1H), 7.95 (d, *J* = 7.8 Hz, 2H)	21.28 (CH_3), 41.82 (CH_2), 46.60 (CH_2), 48.02 (CH_2), 49.36 (CH_2), 64.20 (CHN), 124.43 (CH), 126.69 (CH), 128.50 (CH), 129.21 (CH), 130.06 (CH), 132.29 (CH), 134.41 (CH), 134.64 (Cq), 136.43 (Cq), 137.43 (CH), 138.29 (Cq), 148.42 (Cq), 168.88 (C=O(N)), 193.01 (C=O)	VNK-179 > 95 % purity	Calcd. 347.1760 Observed 347.1766
14 VNK-I-183	93 %		118-122	0.99-1.14 (m, 5H), 1.37 (d, *J*=12 Hz, 2H), 1.53-1.56 (m, 3 H), 1.65-1.68 (m, 1H), 1.77 (d, J=12.6 Hz, 1H), 2.45-2.49 (m, 1H), 7.44 (dd, J=6.6 Hz, J=1.8 Hz 2H), 7.51 (td, J=7.2 Hz, J=1.2 Hz, 1 H), 7.65-7.68 (m, 3 H) 7.93 (d, J=7.8 Hz, 1 H), 7.97 (d, J=8.4 Hz, 2 H).	24.83, 24.89, 25.85, 33.60, 34.97, 124.26, 126.06, 128.73, 128.87, 133.13, 133.28, 134.72, 135.81, 137.30, 138.79, 152.71, 193.50	VNK-183AAA > 95 % purity	Calcd. 352.1468 Observed 352.1466
15	88 %	0.50	Yellow	0.97-1.83 (m, 11H), 2.49 (tt, *J* = 9.6 Hz, *J* = 3.6	24.80, 25.81, 33.45, 34.95, 52.58,	VNK-137	Calcd.

VNK-I-137		Hex/EA 1 : 1	crystals 174-176	Hz, 1H), 5.30 (s, 1H), 7.53 (t, *J* = 7.2 Hz, 1H), 7.65 (d, *J* = 7.2 Hz, 1H), 7.69 (s, 1H), 7.71 (t, *J* = 7.2 Hz, 1H), 7.75 (d, *J* = 8.4 Hz, 2H), 7.94 (d, *J* = 7.8 Hz, 1H), 8.17 (d, *J* = 8.4 Hz, 2H)	55.00, 112.62, 118.67, 124.46, 126.06, 128.95, 131.29, 131.72, 132.16, 132.18, 133.65, 135.12, 137.02, 139.28, 141.44, 152.60, 193.17	> 95 % purity	[M+H] 343.1810 Observed 343.1763
16 VNK-I-169	94 %		162-164	0.94 (m, 2H), 1.04 (m, 3H), 1.24 (d, *J* = 12.6 Hz, 2H), 1.49 (d, *J* = 9.0 Hz, 2H), 1.57 (d, *J* =12.0 Hz, 2H), 2.28 (m, 1H), 5.41 (s, 1H), 7.47 (m, 3H), 7.76 (d, *J* = 8.4 Hz, 1H), 7.84 (s, 1H), 7.87 (d, *J* = 7.8 Hz, 2H), 7.98 (d, *J* = 6.6 Hz, 2H)	24.79, 24.97, 25.83, 34.02, 34.82, 52.85, 55.41, 117.46, 118.50, 124.85, 129.98, 130.53, 130.55, 131.68, 132.35, 134.35, 137.13, 138.26, 140.47, 153.34, 192.31	VNK-169 > 95 % purity	Calcd. [M+H] 343.1810 Observed 343.1808
17 WD compound data	84 %		oil	1.06-1.21 (m, 4H), 1.21-1.34 (m, 2H), 1.59-1.65 (m, 1H), 1.70-1.83 (m, 3H), 1.95-2.05 (m, 1H), 2.45 (dd, *J* = 18.6 Hz, *J* = 3.0 Hz, 1H), 2.60-2.68 (m, 1H), 2.95 (dd, *J* = 6.7Hz, *J* = 18.6 Hz, 1H), 4.52 (dd, *J* = 6.6 Hz, *J*=3.0 Hz, 1H), 7.38 (dd, *J* = 7.3Hz, *J* = 0.9Hz, 1H), 7.59 (dd, *J* = 7.2 Hz, *J* = 0.9 Hz, 1H), 7.63 (d, *J* = 7.7 Hz, 1H), 7.69 (d, *J* = 7.7 Hz, 1H)	24.73, 24.92, 25.94, 33.12, 34.47, 46.01, 53.07, 55.23, 123.14, 125.83, 128.41, 134.73, 136.52, 156.61, 204.77		Calcd. 230.1545 Observed 230.1550
18 VNK-I-146	54 %	0.30 DCM/ MeOH/ NH_4OH 90: 10: 1	oil	1.05-1.30 (m, 6H), 1.49 (d, *J* = 9.6 Hz, 1H), 1.57-1.64 (m, 2H), 1.71-1.77 (m, 1H), 2.01 (d, *J* = 12 Hz, 1H), 2.50-2.56 (m, 1H, *CHN*), 5.15 (s, 1H, *CH*-NCy), 5.77 (s, 1H, *CH*OH), 6.93 (s, 1H), 7.30 (dd, J = 7.8 Hz, J = 7.2 Hz, 1H), 7.31-7.34 (m, 2H), 7.35-7.38 (m, 1H), 7.39 (t, *J* = 7.8 Hz, 2 H), 7.55 (d, *J* = 7.2 Hz, 1H), 7.67 (d, *J* =	25.00 (CH_2), 25.11 (CH_2), 26.10 (CH_2), 32.74 (CH_2), 34.64 (CH_2), 53.25 (CH), 57.49 (CH), 76.25 (CHOH), 124.62 (CH), 125.25 (CH), 126.20 (CH), 127.27 (CH), 128.33 (CH), 128. 38 (CH), 128. 98 (CH), 136.90 (C-q), 143.39 (C-q), 134.61 (C-q), 148.79 (C-	VNK-146 > 95 % purity	Calcd. 320.2014 Observed 320.2004

				7.2 Hz, 2H)	q)		
19 **VNK-108**	47 %		126-129 (decomp.)	**VNK-I-114H:** 0.85-1.80 (m, 15 H), 2.08 (td, *J* = 7.2 Hz, *J* = 2.4 Hz, 2H), 2.25-2.32 (m, 1H), 2.69 (d, *J* = 12.6 Hz, 1H), 2.88 (dd, *J* = 13.2 Hz, *J* = 4.8 Hz, 1H), 3.10 (td, *J* = 7.2 Hz, *J* = 4.8 Hz, 1H), 3.52-3.59 (m, 1H), 4.26 (dd, *J* = 6.0 Hz, *J* = 4.8 Hz, 1H), 4.47 (dd, *J* = 7.8 Hz, *J* = 5.4 Hz, 1H), 5.15 (br. s, 1H), 5.37 (s, 1H), 5.55 (d, *J* = 6.0 Hz, 1H), 5.96 (d, *J* = 17.4 Hz, 1H), 7.39-7.49 (m, 4H), 7.65-7.67 (m, 2H), 7.75 (br.s, 1H), 7.86 (d, *J* = 7.2 Hz, 2H), 7.89 (d, *J* = 7.8 Hz, 1H)	**VNK-I-114CC:** 25.61, 28.00, 29.71, 31.51, 31.61, 32.56, 33.29, 36.02, 40.54, 47.72, 51.74, 55.41, 55.52, 60.12, 61.73, 124.09, 126.13, 128.78, 129.94, 131.36, 134.65, 134.80, 136.25, 137.45, 137.98, 138.03, 152.80 163.48, 172.20, 193.62	VNK-108G > 95 % purity	Calcd. 559.2743, Observed 559.2750
19b	91 %		> 300	**VNK-MT-2_HH:** (D_2O, 600 MHz): δ 1.20-1.65 (m, 7H), 1.75-1.80 (m, 2H), 1.85-1.90 (m, 1H), 1.94-1.99 (m, 1H), 2.02-2.06 (m, 2H), 2.07 (td, *J* = 7.2 Hz, *J* = 3.0 Hz, 1 H), 2.09-2.13 (m, 1H), 2.54 (br.s, 4H), 2.66 (dd, *J* = 13.2 Hz, *J* = 4.2 Hz, 1H), 2.88 (dtd, *J* = 12.6 Hz, *J* = 4.8 Hz, *J* = 1.8 Hz, 1H), 3.08-3.14 (m, 1H), 3.19-3.26 (m, 1H), 3.61-3.65 (m, 3H), 4.32 (ddd, *J* = 13.8 Hz, *J* = 7.8 Hz, *J* = 4.2 Hz, 1H), 4.49 (ddd, *J* = 7.8 Hz, *J* = 5.4 Hz, *J* = 2.4 Hz, 1H)	**VNK-I-105DC:** (DMSO-d6, 150 MHz): δ 26.44, 26.62, 29.30, 29.42, 32.41, 35.37, 35.65, 36.50, 41.29, 50.81, 50.94, 56.70, 60.43, 62.29, 163.95, 174.48		Calcd. 341.2011, Observed 341.2011
20 **VNK-I-211B**	32 %	0.20 Hex/EA 3 : 1	Orange crystals	1.361 (d, 1H, J=12.00), 1.643 (dd, 1H, J=14.40), 1.747 (d, 1H, J=12.60), 2.444 (m, 1H), 3.901 (s,	24.89 (CH_2), 25.89 (CH_2), 33.81 (CH_2), 35.01 (CH_2), 52.46 (CH), 55.41 (CH),	VNK-211 > 95 % purity	Calcd. $[M+H]^+$

			112-113	3H), 5.342 (s, 1H), 6.993 (d, 2H, J=9.00), 7.482 (td, 1H), 7.657 (d, 2H), 7.719 (ds, 1H), 7.918 (d, 1H, J=7.80), 7.952 (d, 2H, J=9.00)	114.15 (CH), 124.06 (CH), 126.02 (CH), 127.44 (CR_3), 128.53 (CH), 133.82 (CH), 134.28 (CH), 135.97 (CH), 137.69 (CR_3), 152.73 (CR_3), 160.98 (CR_3), 193.72 (CO)		348.1964, Observed 348.1907
21 **VNK-I-212**	48 %	0.20 Hex/EA 9 : 1	Yellow oil	0.88-1.10 (m, 8 H), 1.27 (s, 1 H), 1.31-1.50 (m, 2 H), 1.51-1.54 (m, 2 H), 1.60-1.63 (m, 3H), 1.69-1.71 (m, 2H), 2.43 (s, 4H), 5.38 (s, 1H), 7.29 (s, 1H), 7.5 (dt, J= 1.2 Hz, 1 H), 7.65-7.69 (m, 2H) 7.71-7.74 (m, 1H), 7.842 (d, J= 8.4 Hz, 2H), 7.92 (d, J= 7.8 Hz, 1 H)	10.97, 14.07, 21.59, 23.00, 23.73, 24.86, 24.99, 25.86, 28.93, 30.35, 33.85, 34.94, 38.72, 52.50, 55.33, 68.15, 76.81, 77.02, 77.23, 124.09, 126.16, 128.57, 128.81, 128.84, 129.47, 130.90, 131.42, 131.66, 131.96, 132.44, 134.45, 136.04, 137.50, 137.57, 140.25, 140.45, 152.86, 167.78, 193.77	VNK-212 > 95 % purity	Calcd. $[M+H]^+$ 332.2014, Observed 332.0384
22 **VNK-I-215**	66 %	0.16 Hex/EA 9 : 1	Yellow cryslals 131-133	0.94 (m, 2H), 1.04 (m, 3H), 1.24 (d, *J* = 9 Hz, 1H), 1.49 (m, 2H), 1.54 (m, 2H), 1.60 (m, 1H), 2.32 (m, 1H), 5.35 (s, 1H), 7.42 (t, *J* = 7.2 Hz, 1H), 7.47 (t, *J* = 7.2 Hz, 2H), 7.62 (dd, *J* = 8.2 Hz, *J* = 1.8 Hz, 1H), 7.77 (d, *J* = 7.8 Hz, 2H), 7.83 (d, *J* = 1.2 Hz, 1H), 7.87 (d, *J* = 7.2 Hz, 1H)	24.87, 25.01, 25.90, 34.04, 34.89, 52.73, 55.34, 125..54, 128.87, 129.59, 129.89, 130.09, 131.52, 132.35, 134.72, 136.32, 136.85, 137.83, 154.88, 192.66	VNK-215 > 95 % purity	Calcd. $[M+H]^+$ 396.0963, Observed 396.1009
23 **VNK-I-216**	88 %	0.07 Hex/EA 5 : 1	yellow oil	0.88-1.63 (m, 11H), 2.33 (m, 1H), 3.93 (s, 3H), 5.34 (s, 1H), 7.01 (dd, *J* = 8.4 Hz, *J* = 1.8 Hz, 1H), 7.12 (d, *J* = 1.8 Hz), 7.39 (t, *J* = 7.2 Hz, 1H), 7.45 (t, *J* = 7.8 Hz, 2H), 7.70 (s, 1H), 8.85 (t, *J* = 7.8 Hz, 3H)	11.11, 14.21, 23.14, 23.87, 24.97, 25.11, 25.93, 20.07, 30.49, 34.33, 34.95, 38.86, 52.62, 55.65, 55.93, 68.29, 109.86, 116.32, 126.05, 128.16, 128.80, 128.95, 129.58, 131.04, 131.07,	VNK-216 > 95 % purity	Calcd. $[M+H]^+$ 348.1964 Observed 348.1874

					131.17, 134.74, 135.17, 139.09, 156.08, 165.33, 192.19		
24 **VNK-I-217**	88 %		Yellow oil	Mixture of isomers CSA-1-12B – pure, CSA-1-13B – isomerized	ND	Mixture of isomers 20 : 72 by HPLC VNK-217	Calcd. $[M+H]^+$ 292.1701 Observed 292. 1666
25	86 %	0.27 Hex/EA 1 : 1	yellow solid 161-163	0.92-1.12 (m, 5H), 1.30-1.37 (m, 1H), 1.46-1.565 (m, 2H), 1.57-1.68 (m, 3H), 2.3702.45 (m, 1H), 3.88 (s, 3H), 3.94 (s, 3H), 5.28 (s, 1H), 6.98 (d, *J* = 8.4 Hz, 2H), 7.01 (d, *J* = 8.4 Hz, 1H), 7.11 (s, 1H), 7.65 (s, 1H), 7.86 (d, *J* = 8.4 Hz, 1H), 7.88 (d, *J* = 8.4 Hz, 2H)	24.92 (CH_2), 24.99 (CH_2), 25.84 (CH_2), 34.14 (CH_2), 34.99 (CH_2), 52.39 (CH or CH_3), 55.39 (CH or CH_3), 55.50 (CH or CH_3), 55.75 (CH or CH_3), 109.76 (CH), 114.13 (CH), 115.83 (CH), 125.80 (CH), 127.59, 131.13, 133.38 (CH), 134.64 (CH), 136.51, 155.62, 160.72, 164.93, 192.17	> 95 % purity	$(M+H^+)$: Calcd. $[M+H]^+$ 378.2069, Observed 378.2180
26	79 %	0.22 Hex/EA 1 : 1	yellow solid 156-158	2.50 (br.s, 2H), 2.77 (br.s, 2H), 3.62 (br.s, 4H), 3.87 (s, 3H), 3.94 (s, 3H), 5.00 (s, 1H), 6.98 (d, *J* = 8.4 Hz, 2H), 7.02 (dd, *J* = 8.4 Hz, *J* = 2.4 Hz, 1H), 7.07 (d, *J* = 1.8 Hz, 1H), 7.65 (d, *J* = 0.6 Hz, 1H), 7.88 (d, *J* = 8.4 Hz, 1H), 7.95 (d, *J* = 8.4 Hz, 2H)	48.95 (CH_2), 55.38 (CH_3), 55.76 (CH_3), 64.47 (CH), 67.37 (CH_2), 110.97 (CH), 113.92 (CH), 115.71 (CH), 125.96 (CH), 127.66, 131.96, 134.31 (CH), 134.55, 135.87 (CH), 151.15, 160.90, 164.53, 191.78	Purity > 95 % by LC/MS	Calcd. $[M+H]^+$ 366.1705, Observed 366.1795
27	86 %	0.40 Hex/EA 1 : 1	yellow solid 175-177	2.49 (br.s, 2H), 2.75 (br.s, 2H), 3.62 (t, *J* = 4.2 Hz, 4H), 5.08 (d, *J* = 1.2 Hz, 1H), 7.45 (d, *J* = 8.4 Hz, 2H), 7.52-7.56 (m, 1H), 7.65-7.68 (m, 2H), 7.71 (d, *J* = 1.8 Hz, 1H), 7.95 (d, *J* = 8.4	49.03, 64.38, 67.26, 124.41, 126.88, 128.76, 129.20, 133.27, 133.59, 134.42, 135.81, 136.01, 137.03, 138.32, 148.50, 192.90	Purity > 95 % by LC/MS	Calcd. $[M+H]^+$ 340.1104, Observed

				Hz, 1H), 7.97 (d, *J* = 8.4 Hz, 2H)			340.1132
28	77 %		yellow solid 176-178	0.95-1.17 (m, 5H), 1.35 (d, *J* = 12.6 Hz, 1H), 1.47 (s, 1H), 1.51-1.58 (m, 2H), 1.68 (t, *J* = 13.8 Hz, 2H), 2.41 (tt, *J* = 10.2 Hz, *J* = 3.6 Hz, 1H), 5.27 (s, 1H), 7.45 (d, *J* = 8.4 Hz, 2H), 7.64 (dd, *J* = 8.4 Hz, *J* = 1.2 Hz, 1H), 7.69 (d, *J* = 1.8 Hz, 1H), 7.78 (d, *J* = 8.4 Hz, 1H), 7.80 (br.s, 1H), 7.93 (d, *J* = 8.4 Hz, 2H)	24.75 (CH_2), 24.81 (CH_2), 25.78 (CH_2), 33.67 (CH_2), 34.88 (CH_2), 52.55 (CH), 54.99 (CH), 125.52 (CH), 128.95 (CH), 129.28 (CH), 129.86 (C), 132.31 (CH), 133.02 (C), 133.10 (CH), 135.49 (CH), 136.08 (C), 137.99 (C), 154.43 (C), 192.29 (C)	Purity > 95 % by LC/MS	
29	72 %		yellow solid 222-224	2.49 (br.s, 2H), 2.73 (br.s, 2H), 3.62 (br.s, 4H), 5.04 (s, 1H), 7.45 (d, *J* = 8,4 Hz, 2H), 7.67 (d, *J* = 8.4 Hz, 1H), 7.71 (s, 1H), 7.80 (d, *J* = 8.4 Hz, 1H), 7.83 (s, 1H), 7.93 (d, *J* = 8.4 Hz, 2H)	48.99 (CH_2), 64.16 (CH), 67.19 (CH_2), 125.67 (CH), 128.86 (CH), 129.68 (C), 129.96 (CH), 132.76 (CH), 132.98 (C), 133.61 (CH), 136.26 (C), 136.34 (C), 136.58 (CH), 137.14 (C), 150.06 (C), 191.65 (C)	Purity > 95 % by LC/MS	
30	???	0.1 Hex/EA 9 : 1	183-184	2.51 (br s, 2H), 2.74 (br. s, 2H), 3.62 (t, *J*=4.2 Hz, 4H), 5.09 (s, 1H), 7.44-7.50 (m, 3H), 7.66 (d, *J*=1.8 Hz, 1H), 7.79 (d, *J*=.6 Hz, 1H), 7.81 (d, *J*=8.4 Hz, 1H), 7.84 (d, *J*= 6 Hz, 1H), 7.98 (d, *J*=6.6 Hz, 2H)	30.96, 64.22, 67.23, 125.61, 128.57, 129.51, 129.92, 130.22, 132.38, 132.64, 134.57, 135.88, 137.22, 138.09, 150.28, ~192		
31	74 %						
32	72 %						

Table 3. Characterization of bromobenzylidene indanones

Compound	Yield	Rf	Mp, °C	^{1}H NMR ($CDCl_3$, 600 MHz): δ	^{13}C NMR ($CDCl_3$, 150 MHz): δ	HRMS
14a	57 %		168-170 °C	6.38 (s, 1H), 7.55 (d, *J*=1.2 Hz, 2H), 7.57 (t, *J*= 0.6 Hz, 1H), 7.74 (s, 1 H), 7.74 - 7.77 (m, 4H), 7.93(d, *J*=7.8 Hz, 1 H)	42.52, 124.26, 127.07, 129.35, 130.11, 131.93, 133.73, 135.39, 135.67, 135.76, 136.27, 136.94, 150.44, 190.63	Calcd. (M – Br) 253.0420 Observed 253.0339
15a VNK-I-132	83 %	0.60 DCM	Colorless crystals 197-199 (decomp.)	**^{1}H NMR** (DMSO-d6, 600 MHz): δ 7.16 (s, 1H), 7.65 (t, *J* = 7.2 Hz, 1H), 7.74 (s, 1H), 7.83-7.90 (m, 3H), 8.03 (d, *J* = 8.4 Hz, 2H), 8.11 (d, *J* = 8.4 Hz, 2H)	**^{13}C NMR** (DMSO-d6, 150 MHz): δ 43.04, 112.44, 118.49, 123.72, 127.54, 130.44, 132.49, 132.70, 133.83, 135.37, 136.47, 137.54, 138.55, 150.89, 189.90	Calcd. 324.0024, Observed 324.0060
20a VNK-I-211A	28 %		colorless crystals	2.79 (s, 4.6H), 3.92 (s, 3H), 6.397 (s, 1H), 7.06 (d, *J*=8.4 Hz, 2H), 7.78 (d, *J*=7.8 Hz, 1H), 7.84 (d, *J*=9.0 Hz, 2H), 7.91 (d, *J*= 7.8Hz, 1H); 7.53 (t, 1H), 7.72 (t, 2H)	ND	Calcd. $[M-Br]^+$ 249.0916 Observed 249.0723
22a VNK-I-215a	10 %	0.20 Hex/EA 15 : 1	colorless crystals 188-190	6.33 (s, 1H), 7.53 (m, 3H), 7.67 (dd, *J* = 7.8 Hz, *J* = 1.2 Hz, 1H), 7.76 (t, *J* = 5.4 Hz, 2H), 7.82 (d, *J* = 7.2 Hz, 2H), 7.92 (s, 1H)	41.72, 125.59, 129.22, 130.44, 130.54, 131.09, 132.85, 133.39, 133.73, 134.88, 135.26, 137.83, 152.23, 189.87	Calcd. $[M+H]^+$ 376.9171 Observed 376.9174
23a VNK-I-216a	89 %	0.40 Hex/EA 3 : 1	Yellow crystals 146-148	3.95 (s, 3H), 6.34 (s, 1H), 6.05 (dd, *J* = 8.4 Hz, *J* = 1.8 Hz, 1H), 7.16 (d, *J* = 2.4 Hz, 1H), 7.47 (t, *J* = 7.2 Hz, 1H), 7.52 (t, *J* = 7.2 Hz, 2H), 7.68 (s, 1H), 7.81 (d, *J* = 7.8 Hz, 2H), 2H, 7.84 (d, *J* = 8.4 Hz, 1H)	43.08, 56.08, 110.25, 118.17, 126.14, 129.08, 129.88, 130.54, 132.54, 133.78, 135.85, 136.01, 153.52, 165.89, 189.41	Calcd. $[M+H]^+$ 329.0177 Observed 329.0183
25a	91 %		Yellow	3.91 (s, 3H), 3.96 (s, 3H), 6.32 (s, 1H), 7.03-	43.89, 55.48, 55.91, 110.16, 114.52, 117.81,	

			solid 171-173	7.08 (m, 3H), 7.18 (d, *J* = 1.8 Hz, 1H), 7.65 (s, 1H), 7.79 (d, *J* = 8.4 Hz, 2H), 7.84 (d, *J* = 8.4 Hz, 1H)	125.82, 126.32, 129.96, 133.24, 134.69, 135.62, 153.19, 161.52, 165.52, 189.38	
28a	78 %		White solid 199-201	6.29 (s, 1H), 7.52 (d, *J* = 8.4 Hz, 2H), 7.68 (d, *J* = 8.4 Hz, 1H), 7.71 (s, 1H), 7.75 (d, *J* = 8.4 Hz, 2H), 7.78 (d, *J* = 8.4 hz, 1H), 7.93 (s, 1H)	41.23, 125.47, 129.42, 130.33, 130.58, 131.67, 133.70, 133.77, 135.04, 135.11, 136.13, 137.23, 151.90, 189.46	
31a	74 %		White solid 216-219	6.35 (s, 1H), 7.57 (t, *J* = 7.2 Hz, 1H), 7.61 (d, *J* = 8.4 Hz, 1H), 7.64 (d, *J* = 0.6 Hz, 1H), 7.66 (dd, *J* = 8.4 Hz, *J* = 2.4 Hz, 1H), 7.76 (td, *J* = 7.8 Hz, *J* = 0.6 Hz, 1H), 7.79 (d, *J* = 7.8 Hz, 1H), 7.91-7.95 (m, 2H)	41.90, 124.33, 127.12, 130.22, 130.96, 131.27, 133.38, 133.41, 133.79, 134.86, 135.88, 136.13, 136.91, 150.35, 190.34	

Table 4. Characterization of benzylidene indanones

Compound	Yield	Rf	Mp, °C	^{1}H NMR ($CDCl_3$, 600 MHz): δ	^{13}C NMR ($CDCl_3$, 150 MHz): δ	HRMS
25b	99 %		slightly yellow solid, mp = 146-148 °C	3.88 (s, 3H), 3.93 (s, 3H), 3.99 (s, 2H, CH_2), 6.95-7.05 (m, 4H), 7.60 (t, *J* = 1.8 Hz, 1H), 7.64 (d, *J* = 9.0 Hz, 2H), 7.86 (d, *J* = 8.4 Hz, 1H)	32.56, 55.40, 55.68, 109.75, 114.41, 115.08, 126.07, 128.33, 131.67, 132.35, 132.53, 132.94, 152.35, 160.62, 165.03, 192.91	
28b	97 %		white solid 251-254	4.02 (s, 2H), 7.46 (d, *J* = 8.4 Hz, 2H), 7.57-7.62 (m, 3H), 7.65 (t, *J* = 2.4 Hz, 1H), 7.75 (br.s, 1H), 7.79 (d, *J* = 8.4 Hz, 1H)	32.04, 125.75, 129.33, 129.48, 129.90, 131.46, 131.83, 133.25, 133.58, 134.39, 135.98, 136.76, 150.95, 192.92	

Example 15: Structure-Activity Relationship of BCI analogs.

We tested a series of structurally related analogs of BCI in an *in vivo* assay. As described in Molina et al. (Nature Chemical Biology, 2009), Tg(Dusp6:dsEGFP) embryos were treated at 24 hours post fertilization with increasing doses of compounds. After 6 hours treatment, embryos were imaged by the IXU ImageXpress (Molecular Devices), and images were processed by Definiens Software. The software identified bright head structures and measured fluorescence.

In a dose-dependent manner, BCI expanded GFP expression in transgenic embryos and the EC_{50} was measured as 11.4μM (Figure 16). Under similar conditions, BCI-related analogs were tested and EC_{50} values measured. In these studies, MT9 was at least 2.5 fold more potent than BCI, while other analogs were equipotent to BCI (Figure 17).

We next addressed if BCI and related analogs are detrimental to zebrafish embryo survival after prolong exposure. Embryos soaked in BCI at high doses (>10μM) for 24 hours resulted in embryo defects, such as tail necrosis and even death (Figure 17). The percentage of embryos that died after 24 hours treatment was 100% at 20μM. Treatment with the highly potent MT9 resulted in 100% lethality at lower doses (10μM) than BCI. In contrast VNK215, which had similar activity to BCI was non-toxic, even as high as 40μM (Figure 17 and not shown).

Thus, the cyclohexoamino group of BCI appears important for that compound's potency in inhibiting Dusp6 and the addition of a bromine to the indanone group suppresses toxicity.

Example16: BCI Structure-Activity Relationship Studies

Transgenic zebrafish embryos (24 hpf) were treated with 20 μM solution of BCI analogs in 0.5 % aq DMSO and fluorescence photomicrographs were taken after 6 h. The effectiveness of BCI analogs was evaluated by densitometry (ImageJ) of d2EGFP intensity in the dorsal region.

Table 5

Compound	Activity (BCI = 100)	Compound	Activity (BCI = 100)	Compound	Activity (BCI = 100)
1	0	**7**	114	**14**	52
3 (BCI)	100	**8**	Less than BCI	**15**	20
(–)-BCI	156	**9**	114	**16**	Less than BCI
(+)-BCI	82	**10**	27	**17 (ICD)**	0
4	123	**11**	22	**18**	26
5	127	**12**	0	**19**	No activity, trapped in yolk
6	7	**13**	47		

Table 5 shows the *in vivo* activity of eighteen BCI analogs. First, the structural features required for the activity of BCI were determined. Analog **1**, lacking the cyclohexylamine group, and analog **17**

(ICD), lacking the benzylidene group, were inactive. Reduction of the carbonyl group to an alcohol in analog **18** resulted in a significant loss of activity. Thus, for BCI, the amino group and benzylidene are important for the activity of BCI, and the carbonyl group is desirable.

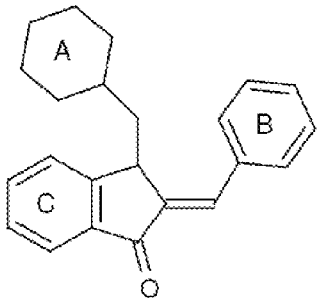

Second, analogs **4-6**, comprising different secondary amines were tested. In reference to the structure above, replacement of ring A of BCI with a cyclopentyl or cyloheptyl ring resulted in a significant increase of activity, whereas replacement of the flexible cyclohexylamine ring with a rigid phenyl group (analog **6**) dramatically decreased activity. Molecular modeling suggested that the NH at C3 of the indanone forms a hydrogen bond with Trp264 in the binding site of Dusp6. To test this hypothesis, we synthesized compound **7**, comprising a piperidine at C3. Unexpectedly, **7** was more active than BCI, despite the lack of a hydrogen bond donor.

Since we established that the group at the C3 of the indanone in the general scaffold can be a secondary or tertiary amine, we studied the effect of additional hydrogen bond donors/acceptors in the 4' position of Ring B of BCI. Introduction of an additional amine in compound **8** resulted in significant loss of activity. Morpholine analog **9** had the same activity as piperidine analog **7**. Thiomorpholine analog **10** and the three piperazine analogs **11-13**, however, had much less activity.

A study of the structure-activity relationship on the periphery of other rings was then undertaken. Molecular modeling suggested that ring B is oriented out of the binding pocket, and substituents on this ring could affect activity only indirectly. We found that introduction of chloride in the *p*-position of ring B resulted in a loss of activity for **14** (52% as compared to BCI), whereas a more electron withdrawing cyano group at this position in **15** decreased activity even further (to 20%). Introduction of a cyano group to ring C in **16** also resulted in a decrease in activity. Finally, biotin-linked analog **19** was completely trapped in the yolk and showed no effect on FGF signaling.

We have separated the enantiomers of BCI by supercritical fluid chromatography over commercially available chiral columns (See, Cole, J., *et al.* Profiling the isomerization of biologically relevant (*E*)-(*Z*) isomers by supercritical fluid chromatography (SFC). *LCGC The Application Notebook – Chromatography Online*, 2009, June 1, 1-6 [erratum in Sept 2009, 51]) and determined that the activity of the levorotatory enantiomer is twice that of the dextrorotatory form. Establishment of the absolute configuration of each enantiomer is in progress.

Having described this invention above, it will be understood to those of ordinary skill in the art that the same can be performed within a wide and equivalent range of conditions, formulations and

other parameters without affecting the scope of the invention or any embodiment thereof. Any document incorporated herein by reference is only done so to the extent of its technical disclosure and to the extent it is consistent with the present application and the disclosure provided herein. Deference is to be given to definitions, descriptions, wording, language, data, statements, *etc.* provided in the present document where any material disclosed in such incorporated references, to include definitions, descriptions, data and statements, conflicts with material provided in the present application.

We claim:

1. A compound having the formula:

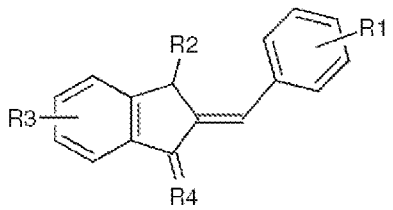

in which R1 represents one or more independently of H, halo, C_{1-3} alkyl, C_{1-3} alkoxyl or –CN; R2 is a primary or secondary amine (-NRH or –NRR', forming, when incorporated into the compound, a secondary or tertiary amine); R3 is one or more independently of H, halo, C_{1-3} alkyl, C_{1-3} alkoxyl or –CN; and R4 is =O or –OH, wherein when R1 and R3 are H and R4 is =O, R2 is not cyclohexylamine, cyclophenylamine, piperidine or morpholine.

2. The compound of claim 1 in which R3 is halo.

3. The compound of claim 2 in which R3 is Br.

4. The compound of claim 1 in which R2 is a C_{4-10} cycloalkylamine.

5. The compound of claim 1 in which R2 is one of cyclopentylamine and cycloheptylamine.

6. The compound of claim 1 in which R1 is H, R2 is one of cyclopentylamine, cyclohexylamine, and cycloheptylamine, and R3 is Br.

7. The compound of claim 6 in which R2 is cyclohexylamine.

8. The compound of claim 1 consisting essentially of a (-) enantiomer of the compound.

9. The compound of claim 1 having the formula:

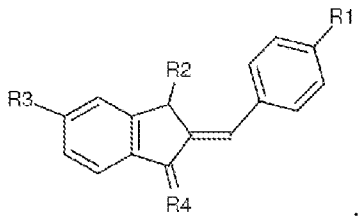

.

10. The compound of claim 1 in which R4 is =O.

11. The compound of claim 10 in which R2 is one of 4-*t*-Boc-cyclohexylamine, thiamorpholine, piperazine, methyl piperazine, acetyl piperazine, cyclopentylamine, cycloheptylamine and di-C_{1-4}-alkylamine.

12. The compound of claim 1 in which R4 is –OH.

13. The compound of claim 1, wherein R1 is 3,4-di-halo.

14. The compound of claim 1, wherein R1 is 3,4-dichloro.

15. The compoound of claim 1, having the structure:

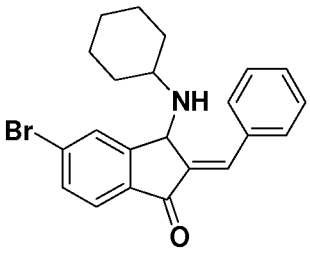

16. A compound consisting of a (-) enantiomer of a compound having the formula:

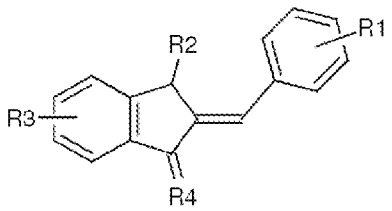

in which R1 represents one or more independently of H, halo, C_{1-3} alkyl, C_{1-3} alkoxyl or –CN; R2 is a primary or secondary amine; R3 is one or more independently of H, halo, C_{1-3} alkyl, C_{1-3} alkoxyl or –CN; and R4 is =O or –OH.

17. A composition comprising one or more compounds of any one of claims 1-16 and a pharmaceutically acceptable excipient.

18. A method of stimulating cell growth in a population of cells, comprising contacting the cell population with compound having the formula:

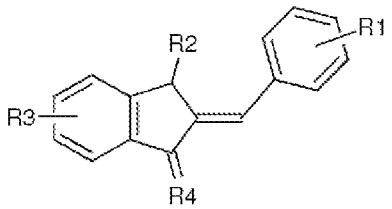

in which R1 represents one or more independently of H, halo, C_{1-3} alkyl, C_{1-3} alkoxyl or –CN; R2 is a primary or secondary amine (-NRH or –NRR', forming, when incorporated into the compound, a secondary or tertiary amine); R3 is one or more independently of H, halo, C_{1-3} alkyl, C_{1-3} alkoxyl or –CN; and R4 is =O or –OH, in an amount effective to increase FGF secretion by the cell.

19. The method of claim 18, comprising applying the compound to a tissue in an organism.

20. The method of claim 19 in which the tissue of the organism is damaged or deficient.

21. The method of claim 18 comprising obtaining cells from a patient and contacting the cells *in vitro* with the compound to expand the population of cells.

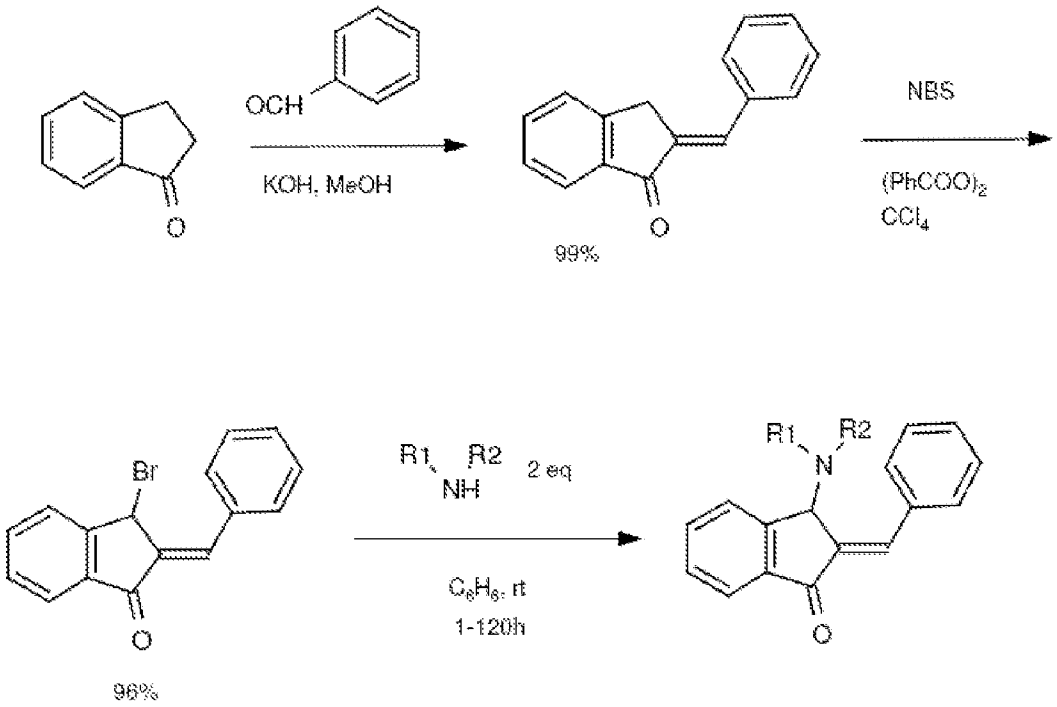
OCH
KOH, MeOH
99%
NBS
(PhCOO)2
CCl4
Br
96%
R1 R2
NH
2 eq
C6H6, rt
1-120h
N

Fig. 1

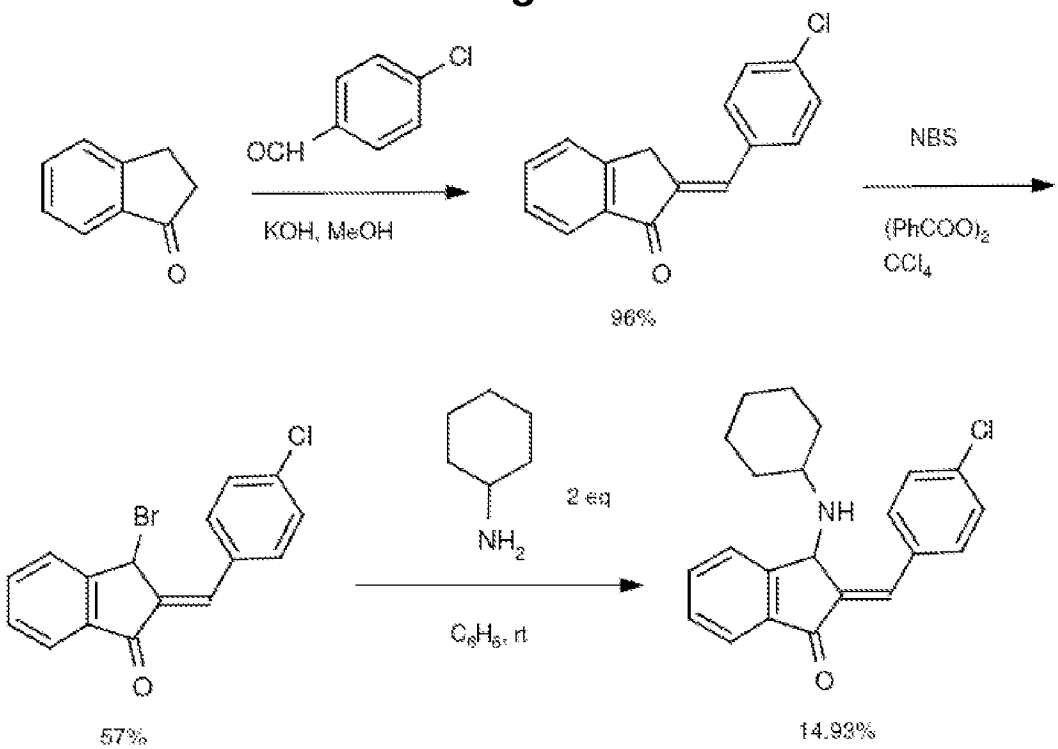
Cl
OCH
KOH, MeOH
96%
NBS
(PhCOO)2
CCl4
Br
57%
NH2
2 eq
C6H6, rt
NH
14.93%

Fig. 2A

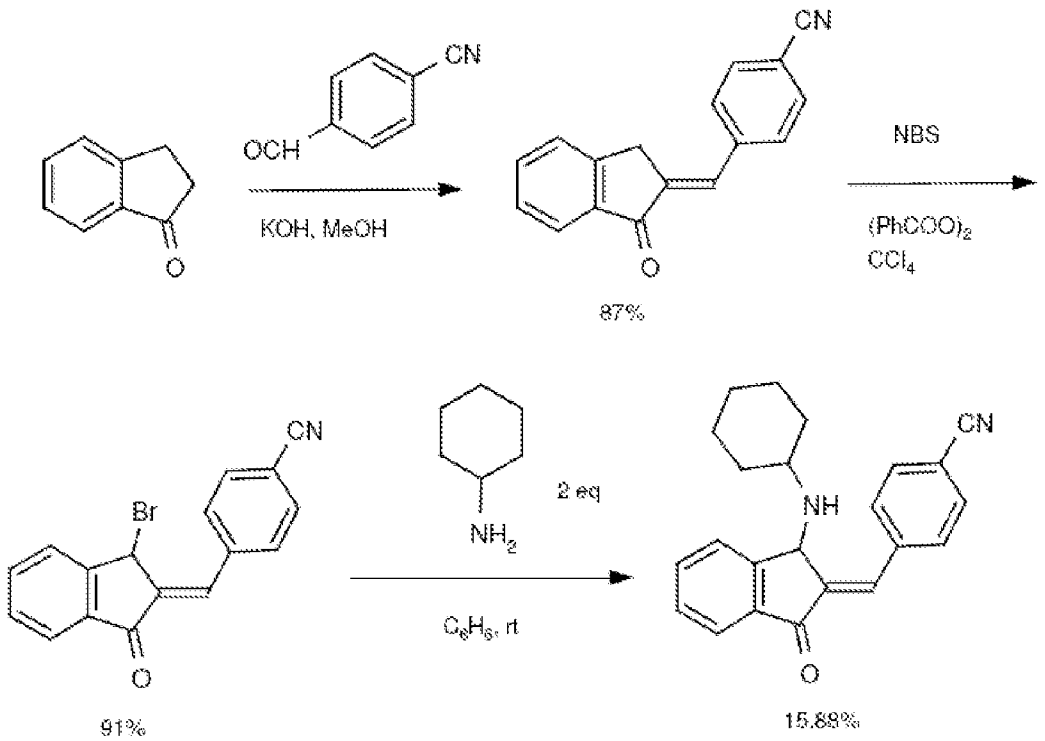
CN
OCH
KOH, MeOH
87%
NBS
(PhCOO)2
CCl4
Br
91%
2 eq
NH2
C6H6, rt
NH
15.88%

Fig. 2B

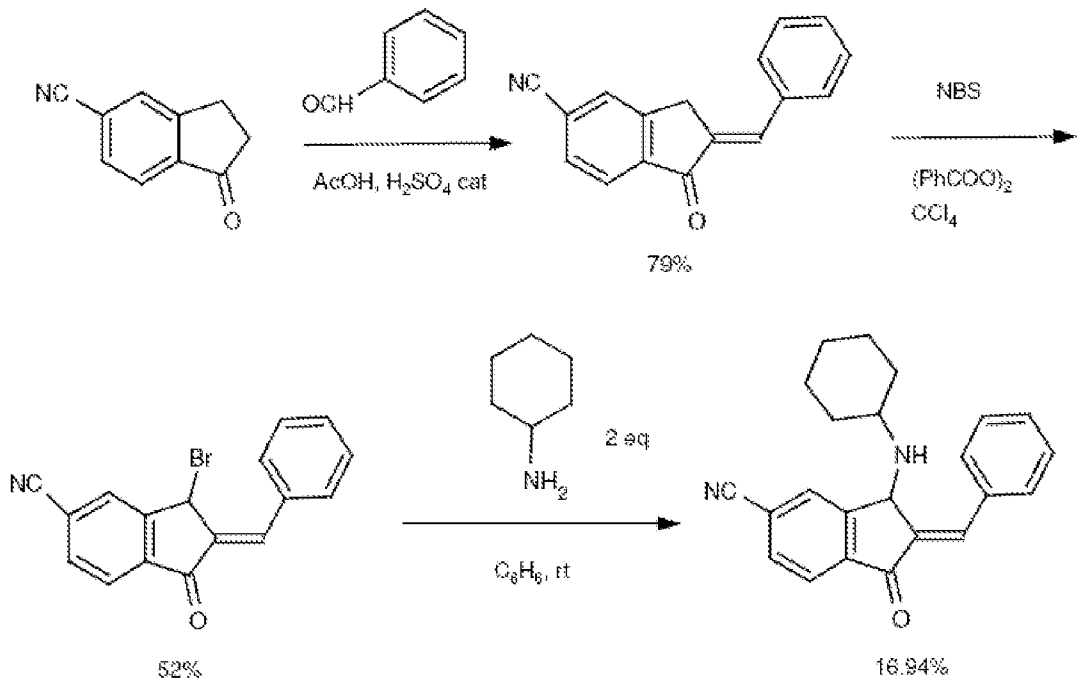
NC
OCH
AcOH, H2SO4 cat
79%
NBS
(PhCOO)2
CCl4
Br
52%
2 eq
NH2
C6H6, rt
NH
16.94%

Fig. 2C

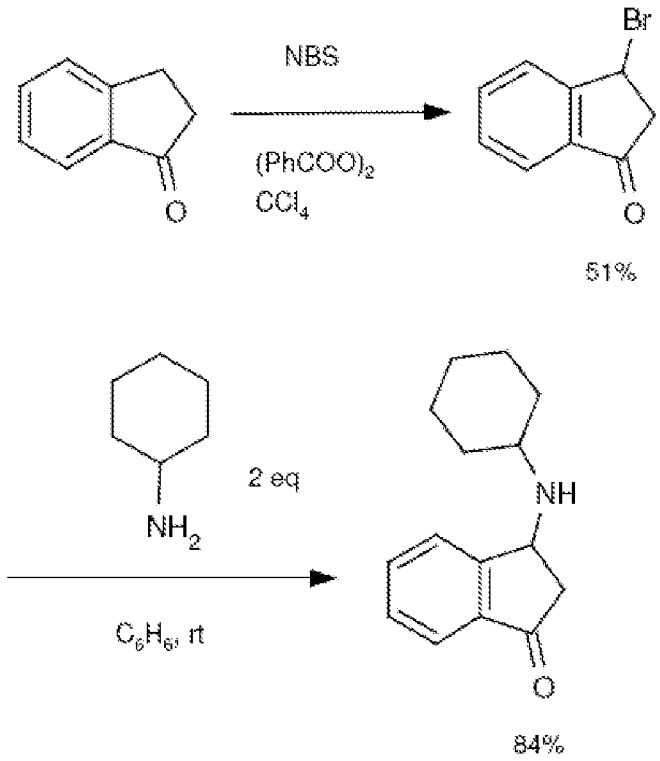
NBS
(PhCOO)2
CCl4
Br
O
51%
2 eq
NH2
C6H6, rt
NH
O
84%

Fig. 3

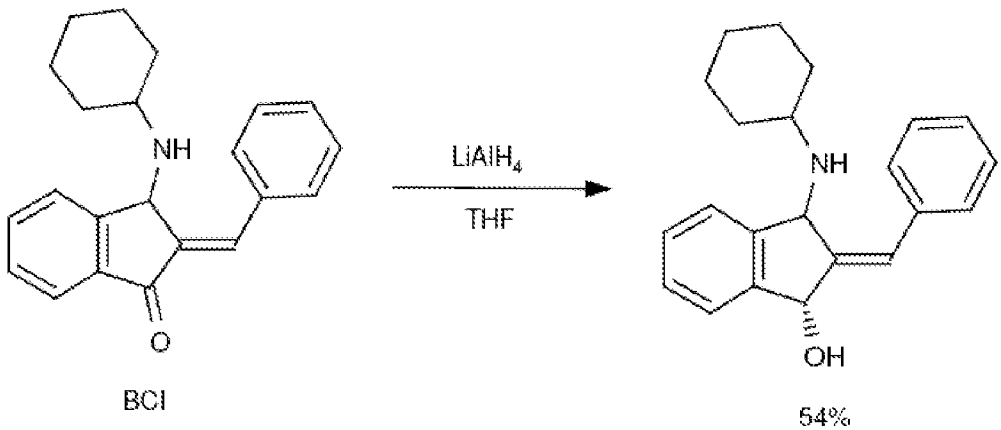
NH
O
BCI
LiAlH4
THF
NH
OH
54%

Fig. 4

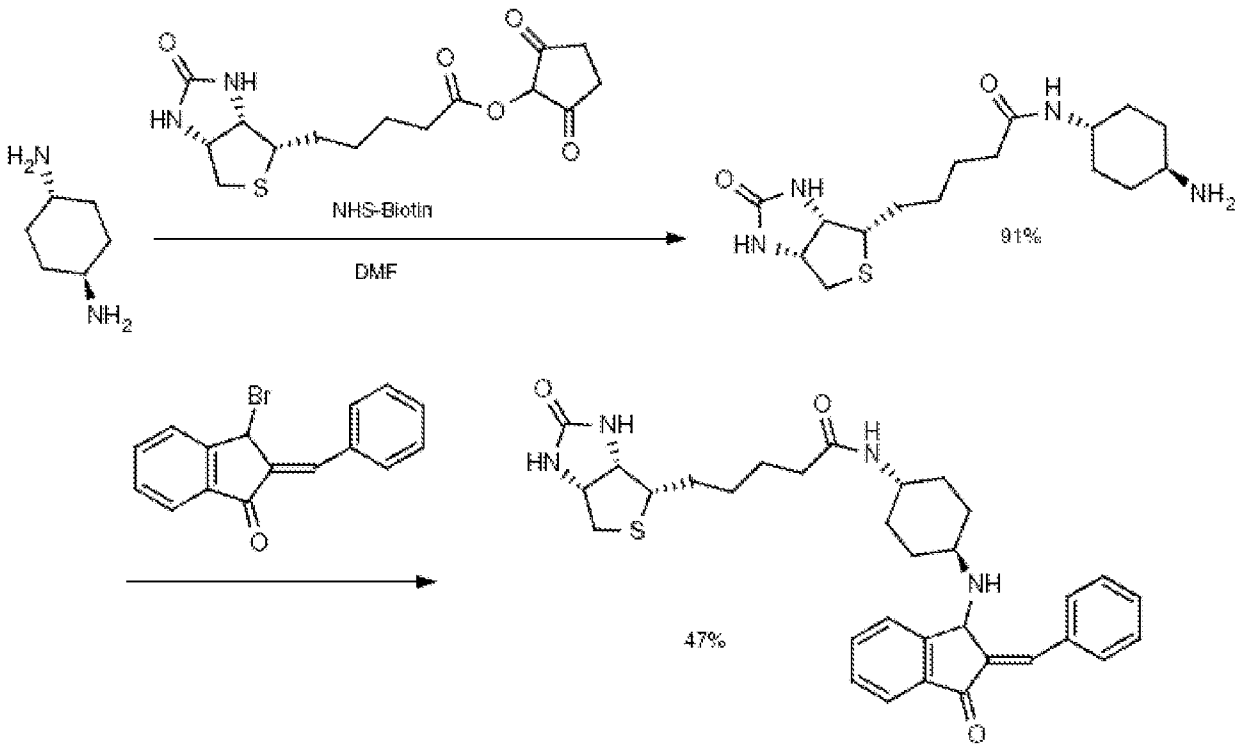

Fig. 5

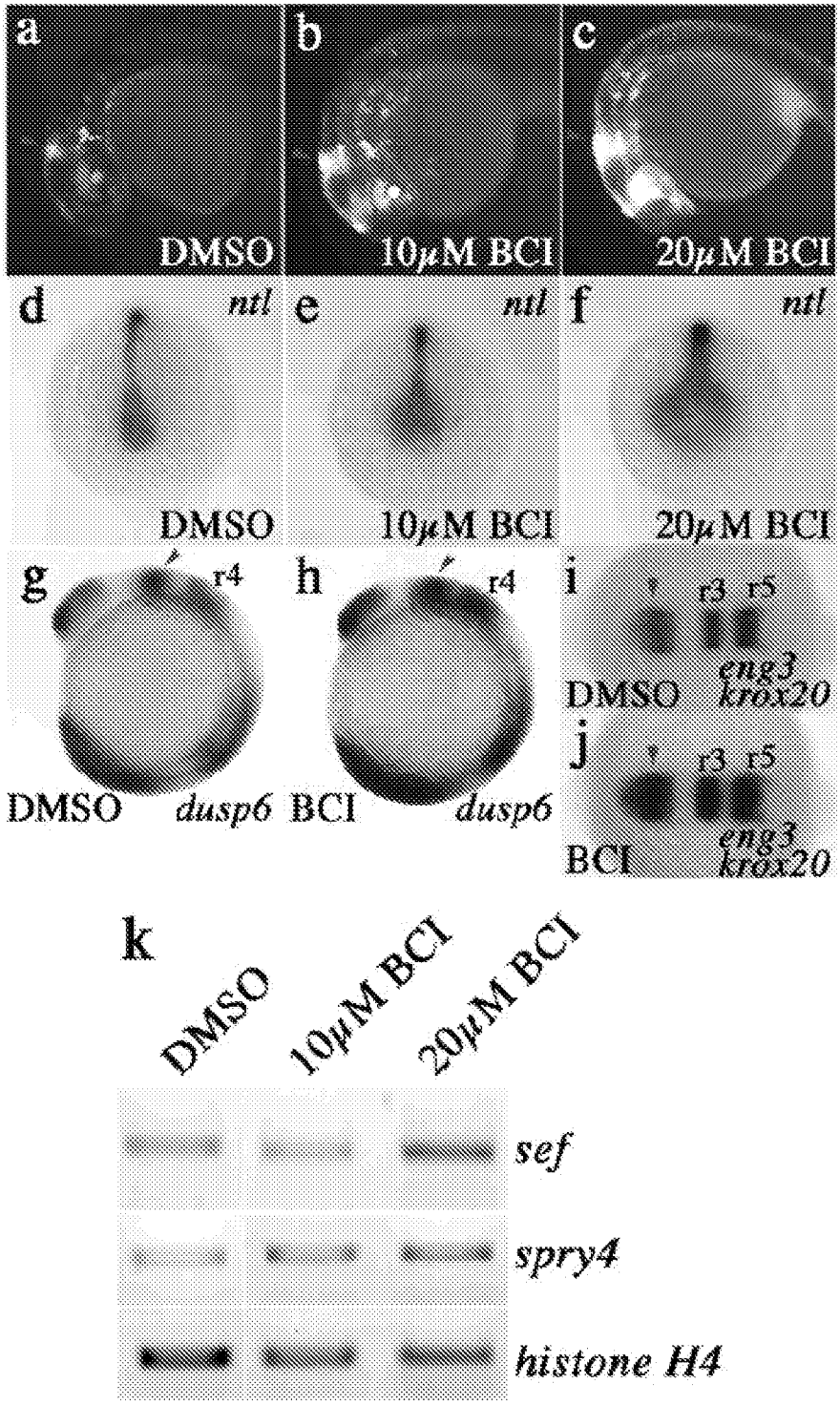
a
DMSO
b
10μM BCI
c
20μM BCI
d
ntl
DMSO
e
ntl
10μM BCI
f
ntl
20μM BCI
g
r4
DMSO
dusp6
h
r4
BCI
dusp6
i
r3
r5
eng3
DMSO
krox20
j
r3
r5
eng3
BCI
krox20
k
DMSO
10μM BCI
20μM BCI
sef
spry4
histone H4

Fig 6

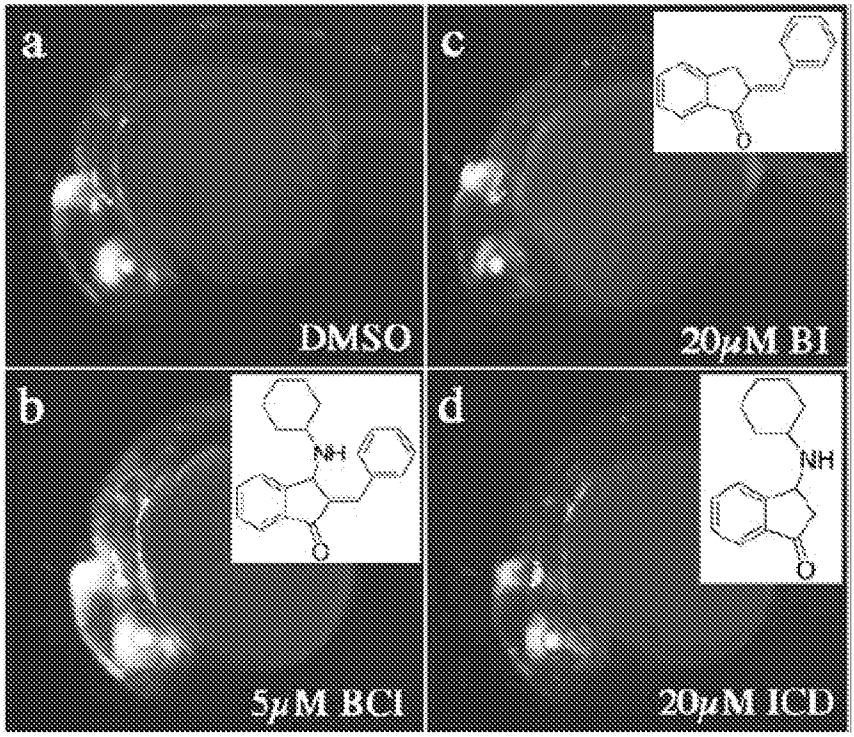

Fig. 7

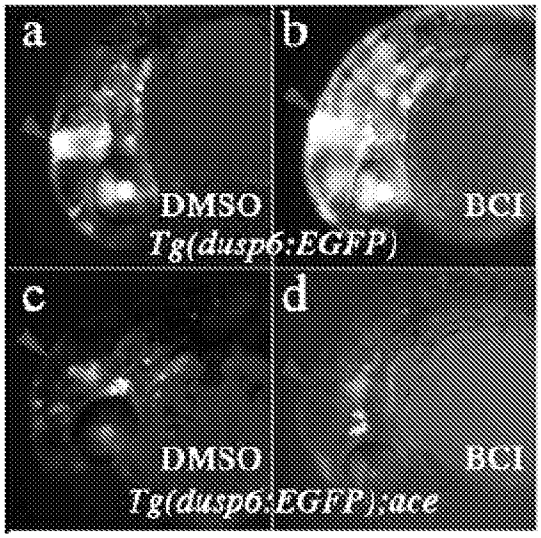

Figs. 8a-d

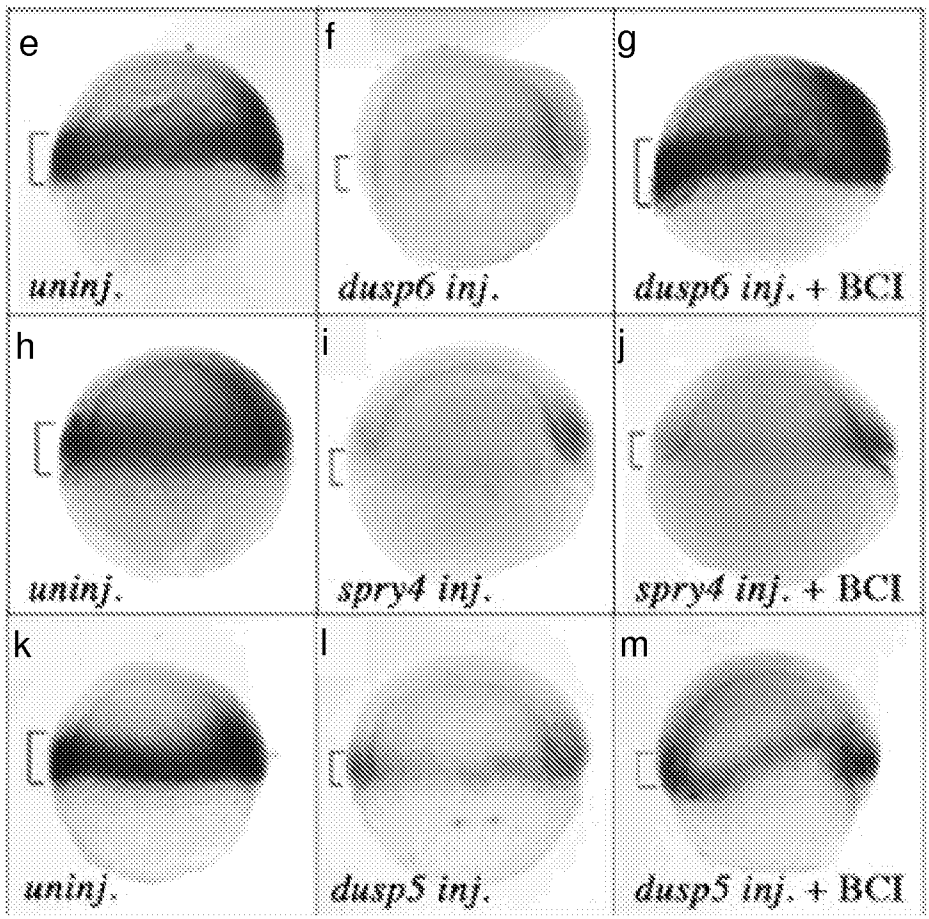

Figs. 8e-m

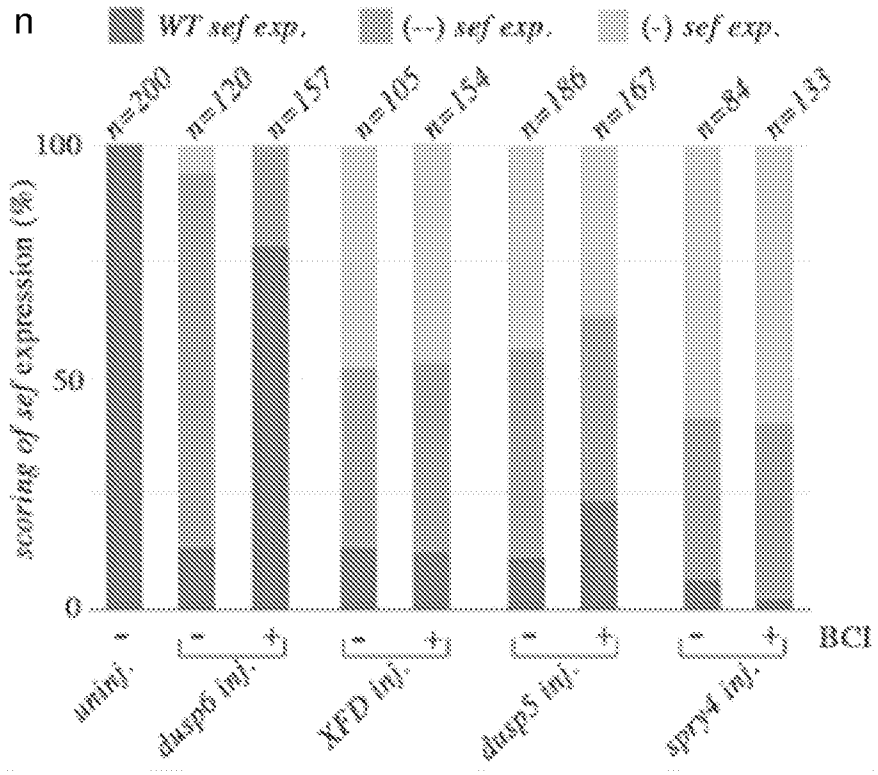
n
WT sef exp.
(--) sef exp.
(-) sef exp.
n=280
n=130
n=157
n=105
n=154
n=186
n=167
n=84
n=133
100
50
0
scoring of sef expression (%)
-
-
+
-
+
-
+
-
+
BCI
uninj.
dusp6 inj.
XFD inj.
dusp5 inj.
spry4 inj.

Fig. 8n

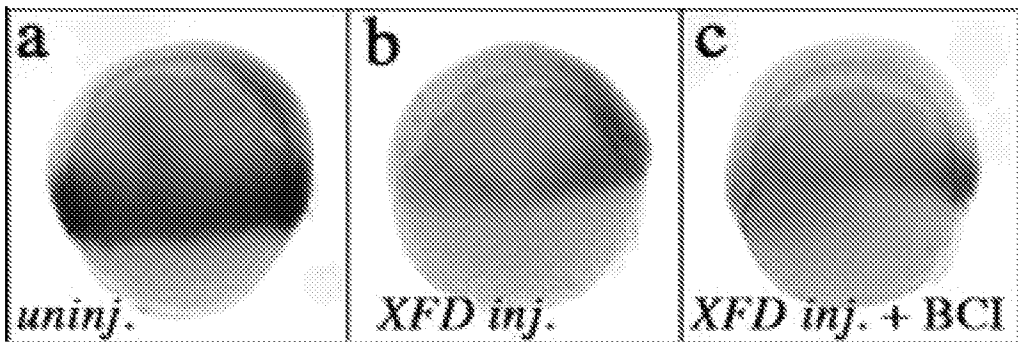
a
uninj.
b
XFD inj.
c
XFD inj. + BCI

Fig. 9

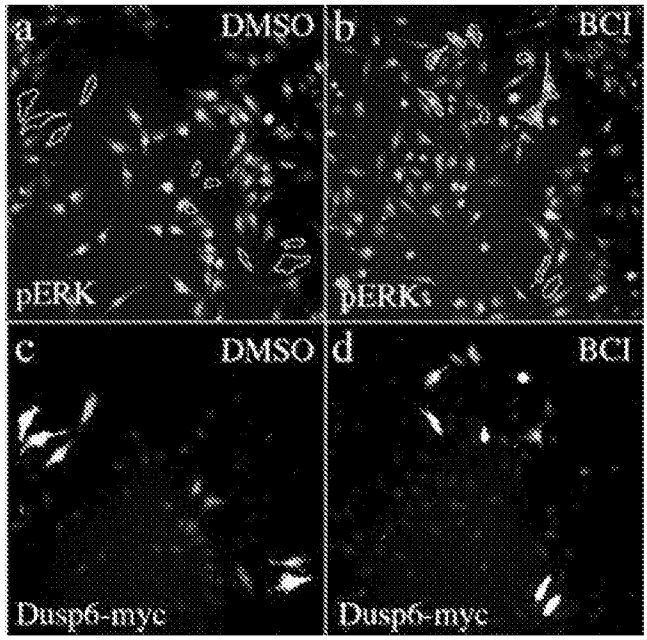

Figs. 10a-d

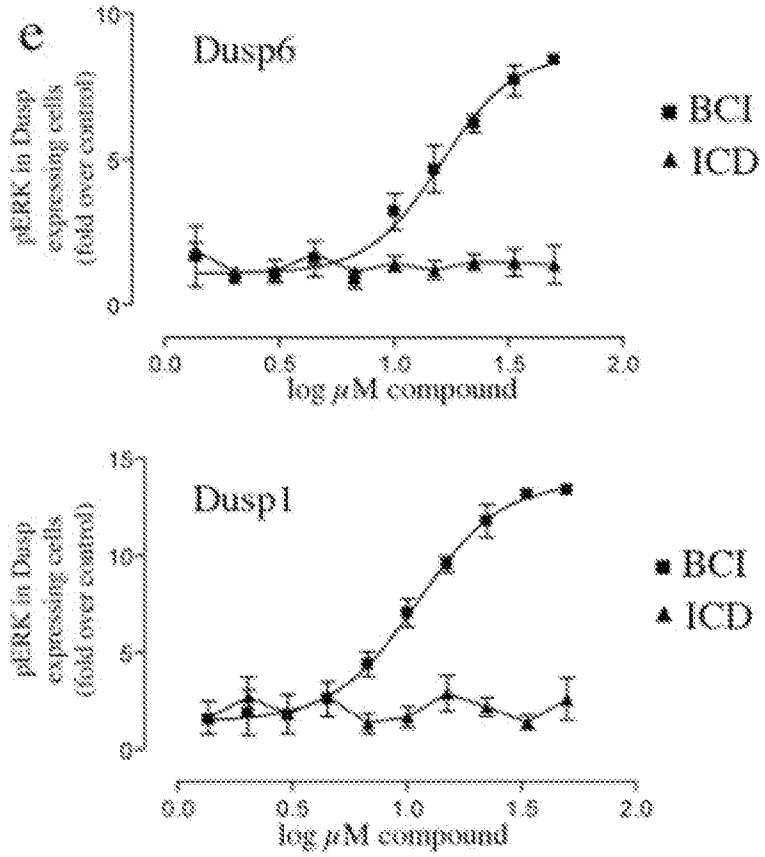

Fig. 10e

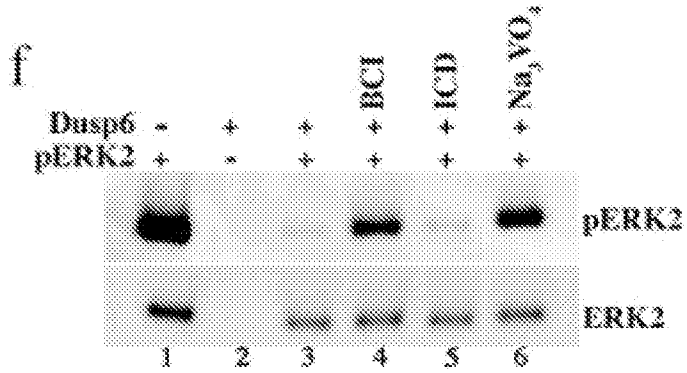

Fig. 10f

Cdc25B

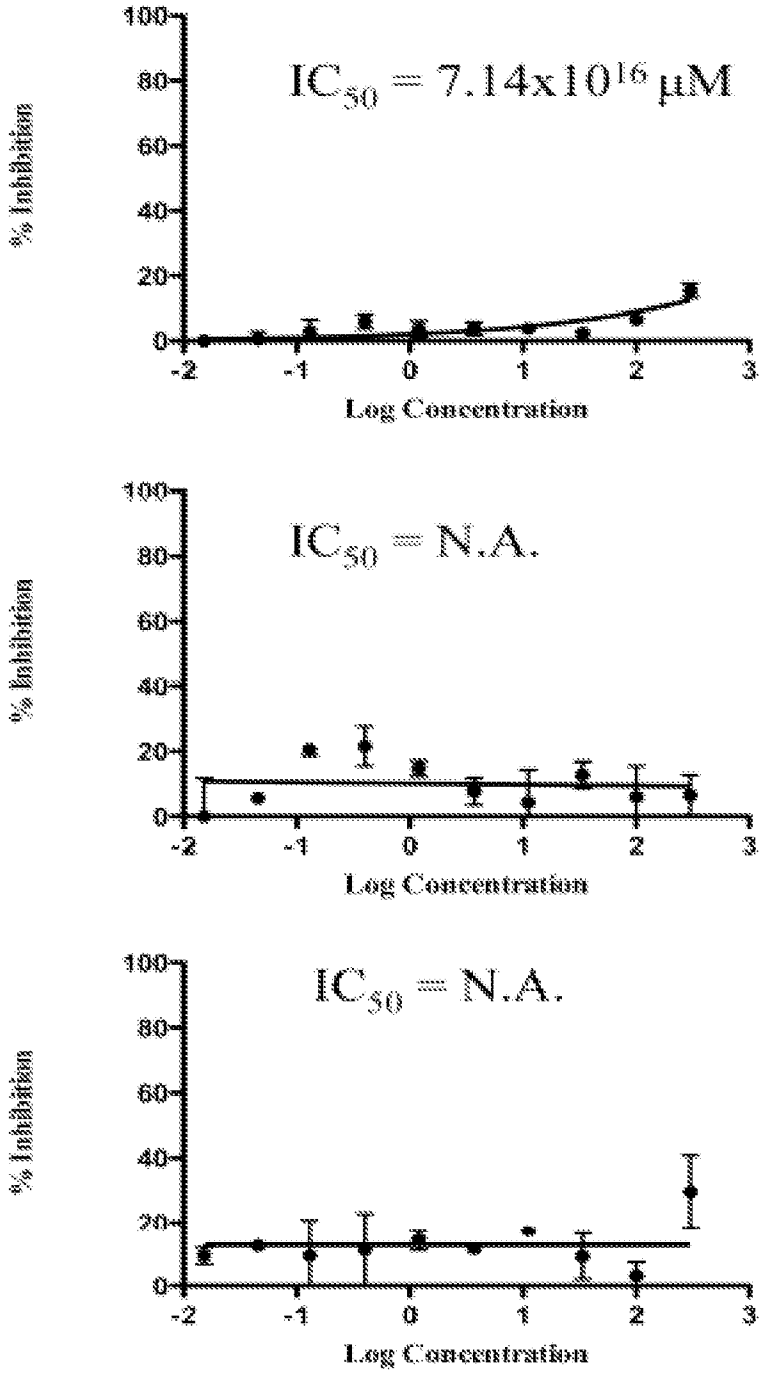

Fig. 11A

PTP1B

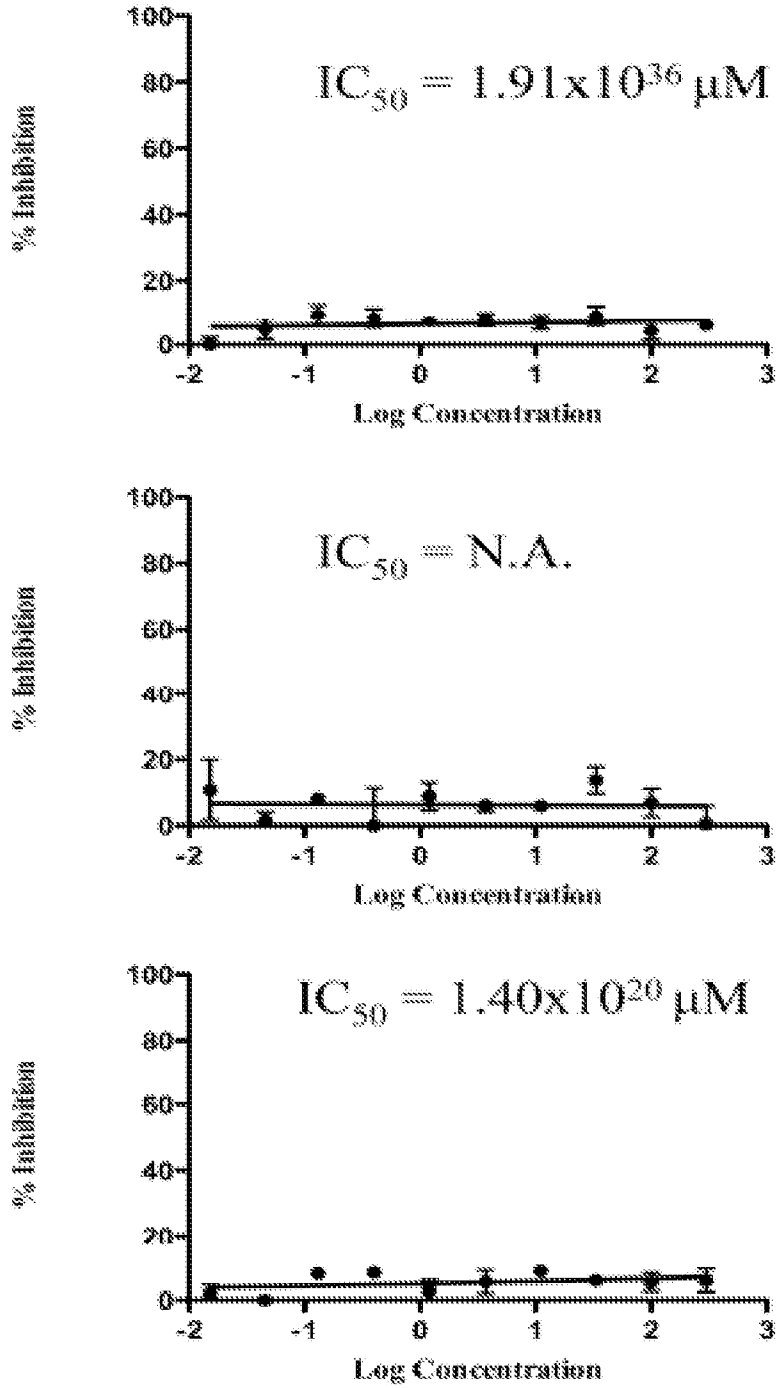

Fig. 11B

VHR

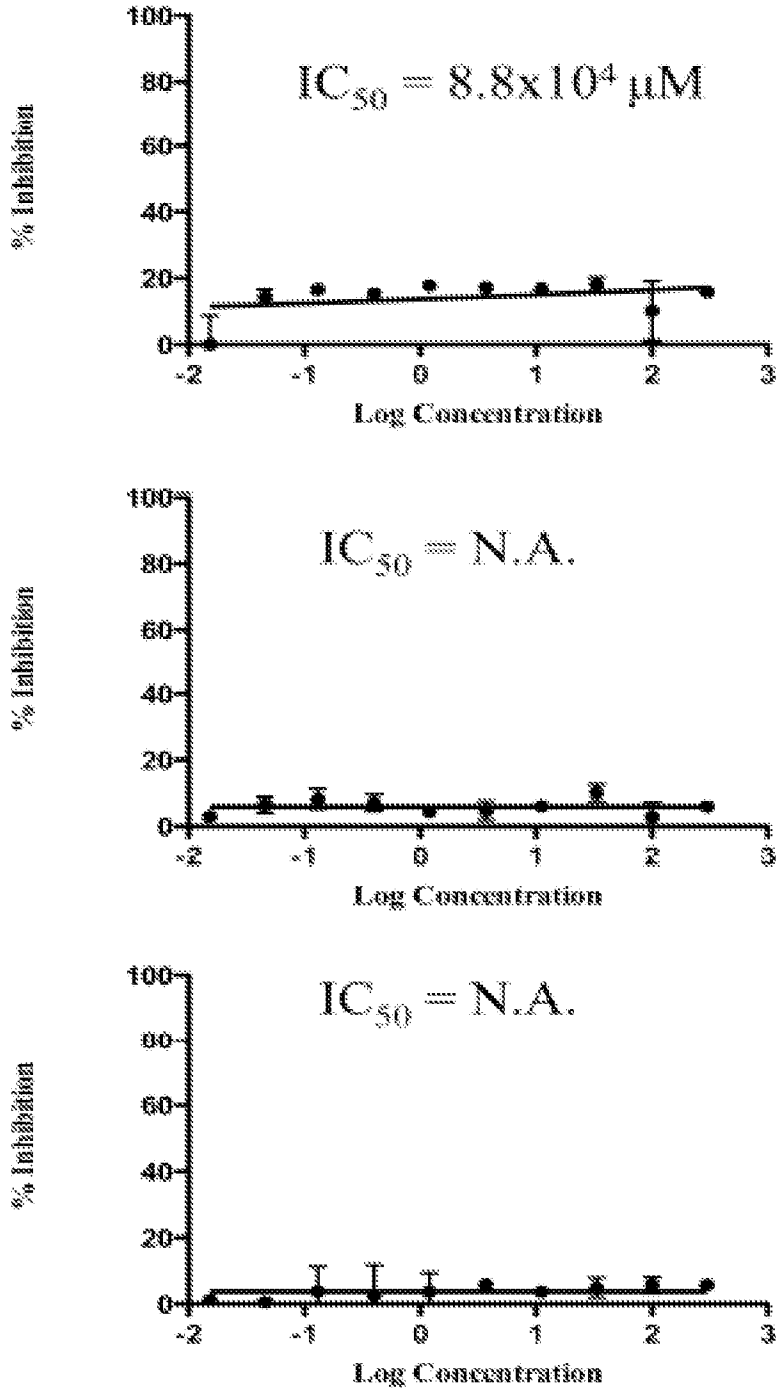
IC50 = 8.8x10^4 µM
% Inhibition
Log Concentration
IC50 = N.A.
% Inhibition
Log Concentration
IC50 = N.A.
% Inhibition
Log Concentration

Fig. 11C

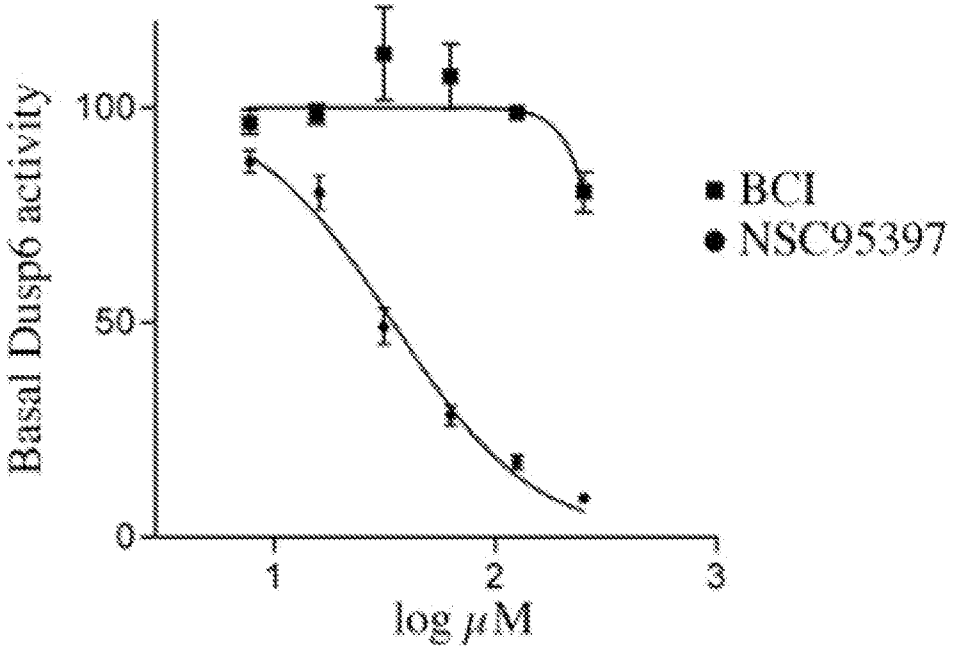

Fig. 12A

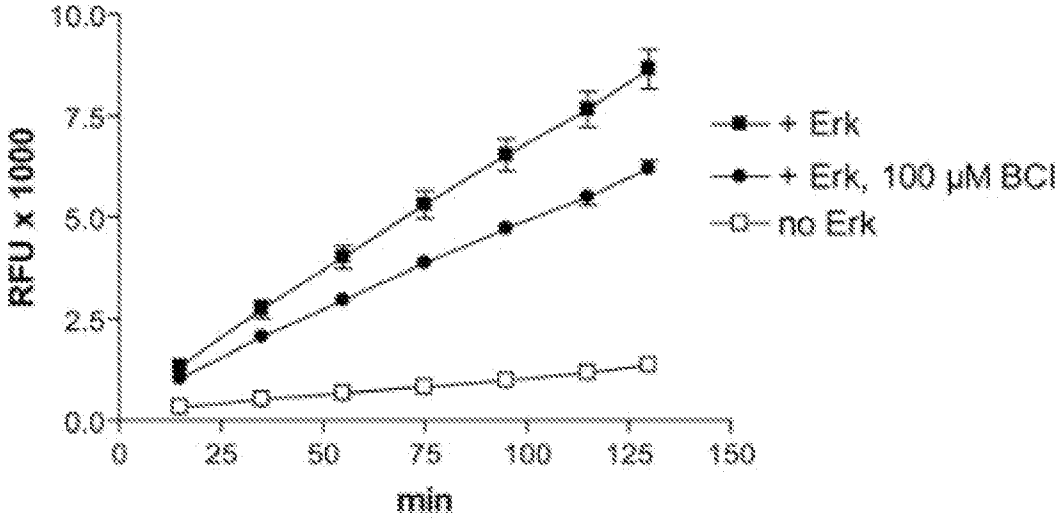

Fig 12B

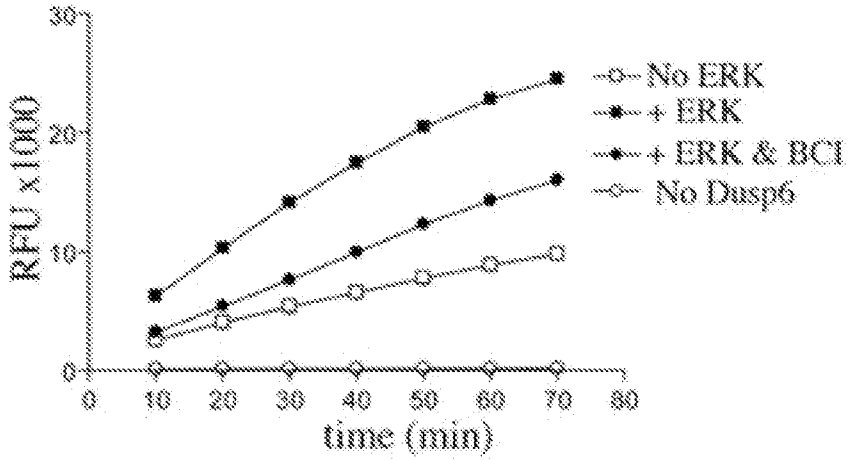

Fig. 13

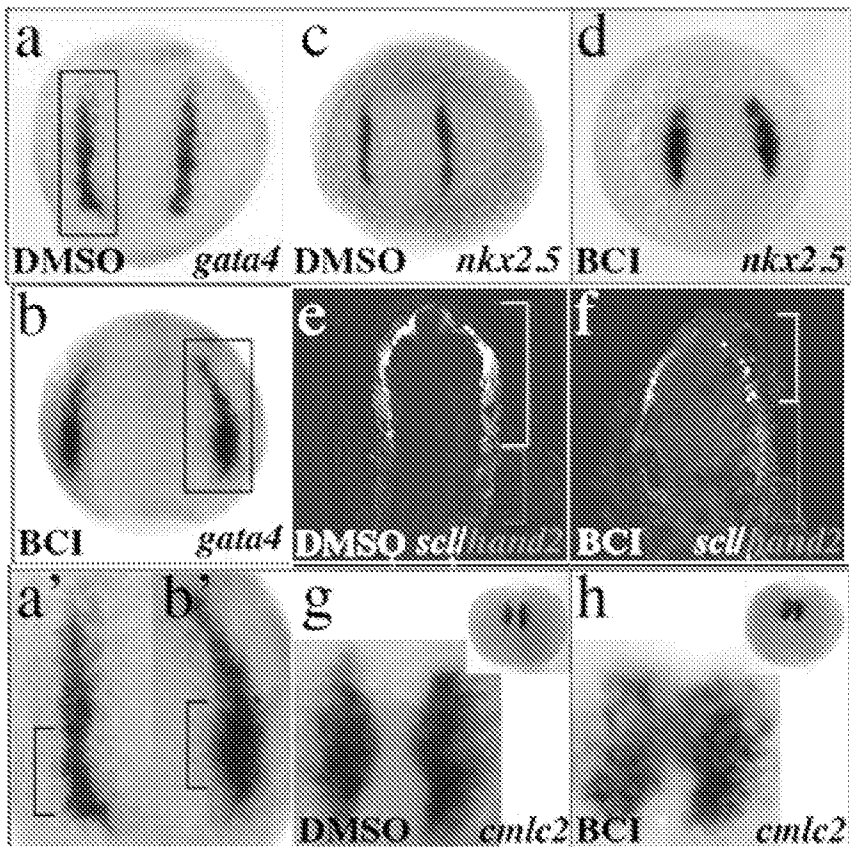

Figs. 14a-h

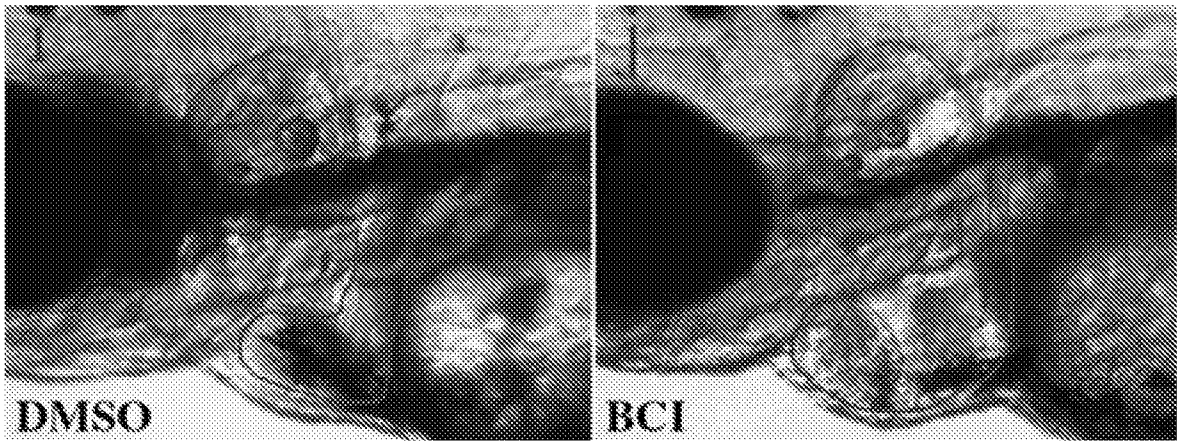

Figs. 14i-j

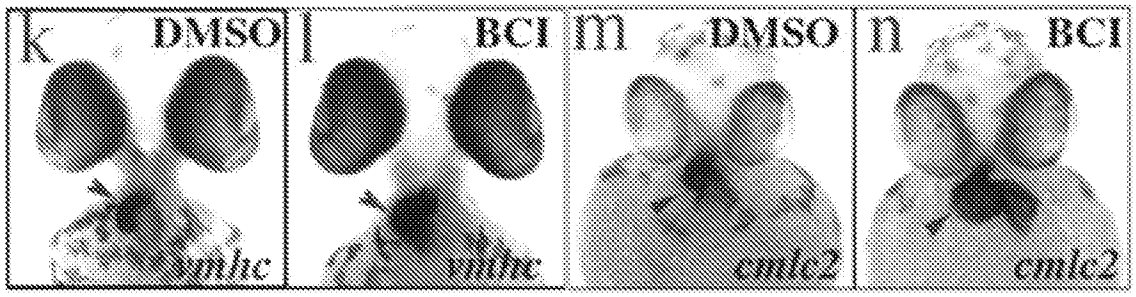

Figs. 14k-n

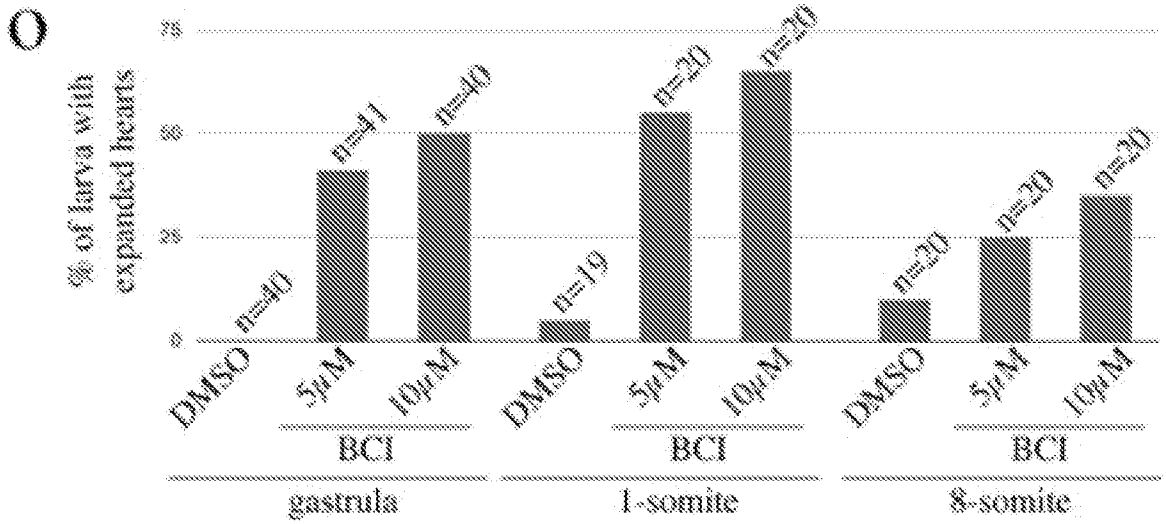

Fig. 14o

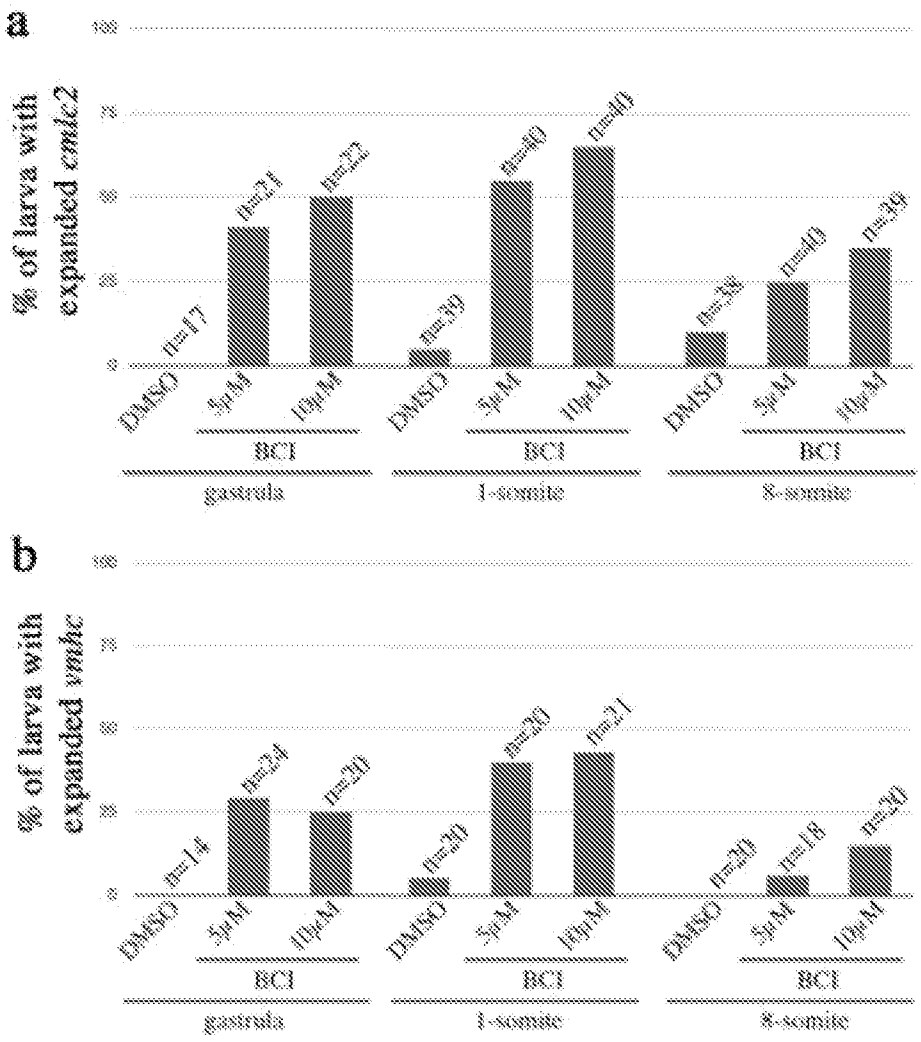
a
% of larva with expanded cmlc2
n=17
n=21
n=22
n=39
n=60
n=40
n=38
n=40
n=39
DMSO
5μM
10μM
BCI
gastrula
1-somite
8-somite
b
% of larva with expanded vmhc
n=14
n=24
n=20
n=30
n=30
n=31
n=20
n=18
n=20

Fig. 15

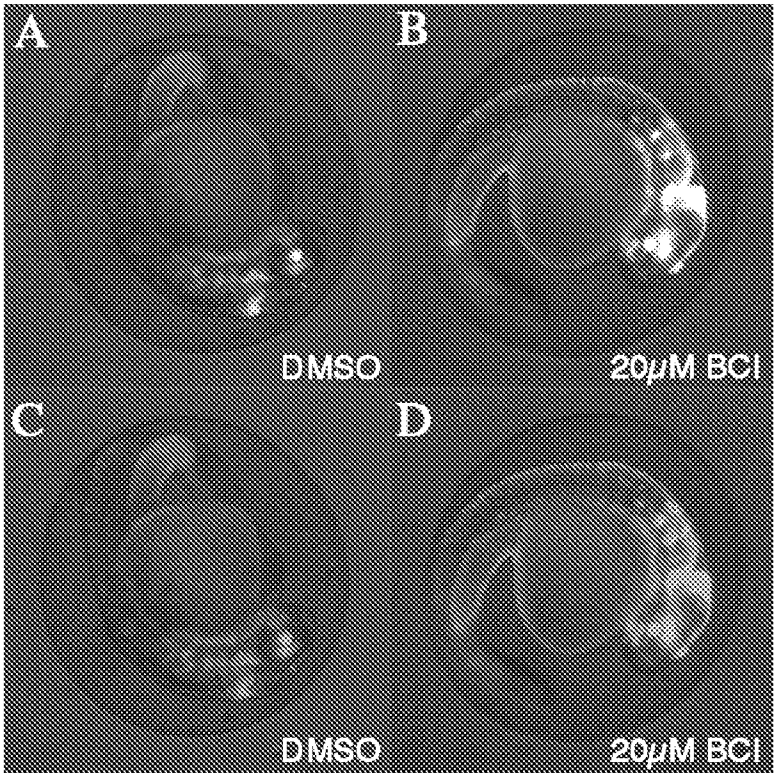

Fig. 16

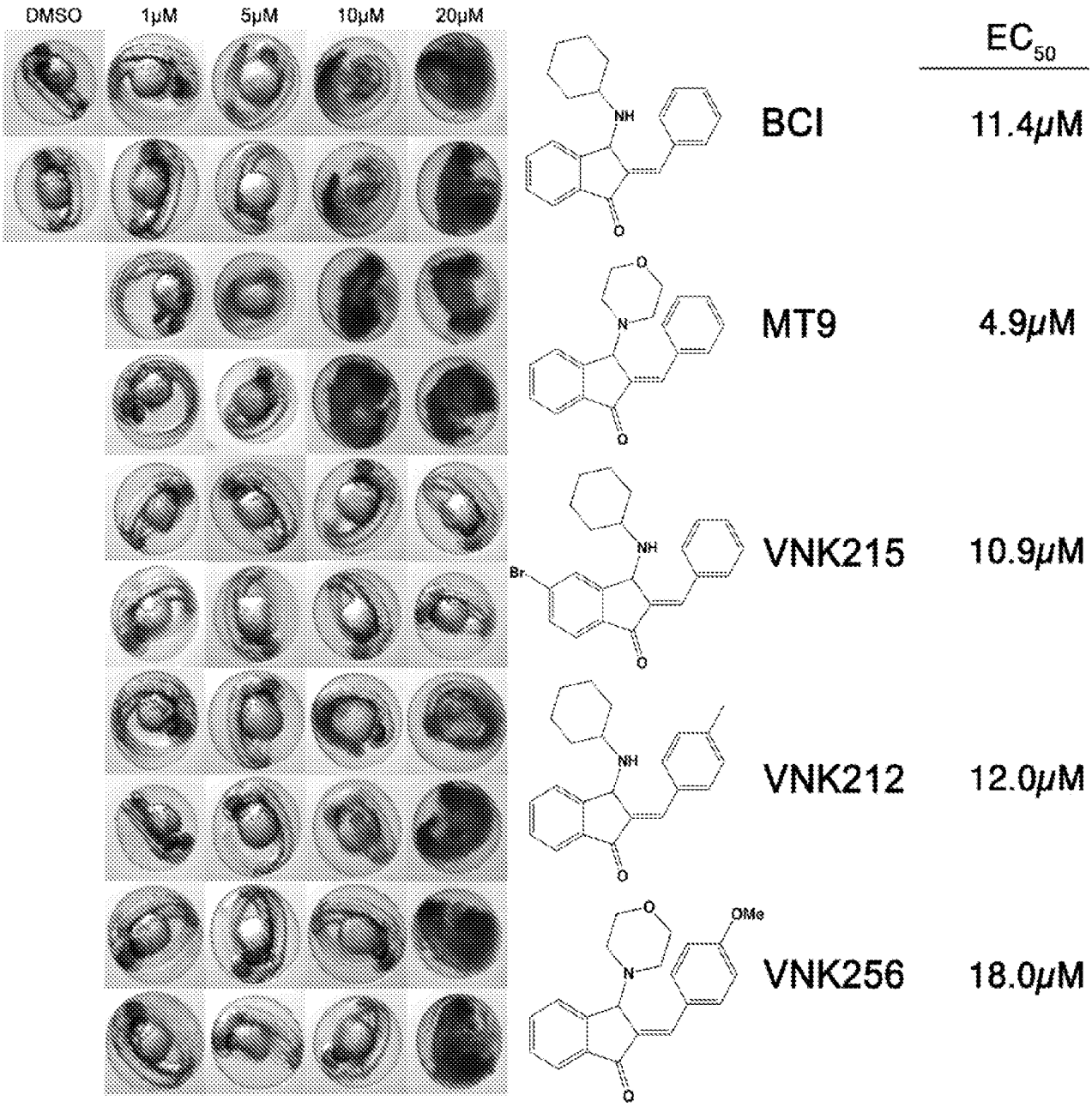
DMSO
1μM
5μM
10μM
20μM
EC50
BCI
11.4μM
MT9
4.9μM
VNK215
10.9μM
VNK212
12.0μM
VNK256
18.0μM

Fig. 17